



Cite this: *Phys. Chem. Chem. Phys.*,
2022, **24**, 24614

Trends in angle-resolved molecular photoelectron spectroscopy

Danielle Dowek^{*a} and Piero Decleva ^{*b}

The field of angle-resolved molecular photoelectron spectroscopy is reviewed, with emphasis on foundations and most recent applications in different regimes of light–matter interaction. The basic formalism underlying one-photon electron angular distributions is presented, from the primary molecular frame (MF) photoemission *i.e.* emission from fully oriented molecules to laboratory frame (LF) observables produced from randomly oriented targets, extensions to multiphoton and strong field processes being briefly described, followed by a survey of current quantum mechanical computational approaches. The description of experimental developments is focused on the advancements in two major instrumentation fields for angle-resolved PES of molecules in the last two decades, namely charged-particle imaging spectrometers and adiabatically or impulsively laser-induced molecular alignment, together with their interplay with the remarkable characteristics achieved nowadays by the ionizing light sources and the challenging control of complex molecules in the gas phase. Aspects and applications of LF angular observables from unoriented targets are presented, with contemporary applications, especially as probes of the target electronic structure, including higher angular observables, in particular photoelectron circular dichroism (PECD) from chiral molecules, which is confirmed as a powerful chiral technique, and higher terms arising from multiphoton or non-dipole terms. Molecular frame photoelectron angular distributions (MFPADs), which stand out as the most complete observables of molecular photoionization stereodynamics in different excitation regimes, now broadly extended to characterize molecular structure and dynamics, are then discussed stemming from fully oriented molecules tackled by electron–ion momentum coincidence techniques, or from laser aligned samples. Finally, novel developments and challenging perspectives, notably the implementation of PAD in time-resolved schemes at ultrashort time scales, high energy, and high intensity regimes are drawn.

Received 15th June 2022,
Accepted 8th August 2022

DOI: 10.1039/d2cp02725a

rsc.li/pccp

Introduction

Over a century has passed since the discovery of the photoelectron effect by Hertz and Lenard, and the explanation by Einstein in terms of photons, alternating periods of slow developments and quantum leaps. These were basically determined by the emergence of new light sources and new spectrometers and detectors. The modern era of photoelectron spectroscopy was ushered by Siegbahn and Turner, with the introduction of bright fixed wavelength sources in the X-ray and VUV regions, and high resolution electron spectrometers. A second step was the developments of dedicated synchrotrons, and widespread use of coincidence detection. The current one is marked by the advent of powerful lasers, and free electron lasers (FEL), and further improvement of detectors able to collect the full 4π emission.

This has allowed probing the photoionization process in amazing detail, in the three directions of photon energy, field intensity and time resolution. This perspective will be focused on angularly resolved molecular photoionization studies, that is photoelectron angular distributions (PADs), and especially studies with fixed in space molecules molecular frame PADs (MFPADs), in the one photon, multiphoton and strong field regimes, but we only briefly touch the time domain aspects, which are addressed in a companion paper.¹ The lack of spherical symmetry of the molecular potential generates a large number of partial waves in the continuum, whose interference is reflected in the MFPADS, but gets averaged for random orientation. There are several motivations for the continuing intense study of these processes. The basic one is the detailed understanding of light–matter interaction at energies above ionization. It is worth recalling that the largest part of the total oscillator strength for electronic excitation generally lies in the continuum. While the basic theory of molecular PADS was fully developed,² and later expanded to cover nondipole effects at higher energies, the description of the interaction with molecular electronic structure, especially the continuum, and the

^a Université Paris-Saclay, CNRS, Institut des Sciences Moléculaires d'Orsay, 91405 Orsay, France. E-mail: danielle.dowek@universite-paris-saclay.fr

^b CNR IOM and Dipartimento DSCF, Università di Trieste, Trieste, Italy. E-mail: decleva@units.it



nuclear degrees of freedom is a big challenge which is still advancing. Correlation and relativistic effects, multichannel scattering and resonances, vibrational excitation and dissociation, and the coupling of electronic and nuclear motions are all topics of current research, for which photoionization has been the most powerful probe. At the most basic level quantum interference and entanglement are still generating surprising effects. As an instrument for studying properties of molecular targets, photoionization continues to give ever finer details of the structure and the dynamics, thanks to the availability of ultrafast pulses in time resolved studies, for which photoionization is one of the most effective probes. Coincidence detection of fragment ions adds a further dimension. Also the range of targets is expanding, from prototypical small molecules to large systems of chemical or biological interests, clusters, and nanoparticles, thanks to the development of powerful methods to bring intact molecules in the gas phase, now extending to adsorbates and liquids.

The combination of selection of orbital ionization, photon energy dependence and angular information, already for randomly oriented molecules up to the MFPADS, offers an enormous amount of information which is becoming available even for complex targets, relying on many current developments extending the technique of molecular alignment and orientation *via* laser pulses and external fields.

This perspective will start with a review of the formalism of PADS, and of the theoretical tools for their simulation by electronic structure calculations. Some current experimental methods will be then described. Present capabilities will be illustrated through a discussion of selected latest studies, first relative to PADS from randomly oriented molecules and the information that can be gained, focusing in particular on chiral systems and high energy experiments, and then from full MFPADS or molecular alignment. Finally a glimpse of near future developments will be given.

Formalism

The formulation of angular distribution in all generality is relatively involved, so we shall follow the simplest path and indicate generalizations. It was first derived by Dill² and further considered by many authors.^{3–8} One needs to define a molecular frame (MF) fixed with the molecule, with axis (X, Y, Z) (in general unprimed quantities), and a laboratory frame (LF) (X', Y', Z') (primed quantities).

Light propagation and polarization are defined in LF, molecular quantities in MF. The Euler angles $\Omega \equiv \alpha, \beta, \zeta$ define the rotation $\text{MF} \rightarrow \text{LF}$, and the photoelectron momentum is k with emission angles θ, φ in MF as shown in Fig. 1, with corresponding θ', φ' in LF. In the simple case of linear (LP) or circular (CP) polarization, the field is defined by a single vector (electric polarization with LP, propagation direction for CP) generally chosen as Z' axis in LF, and therefore on (β, α) as polar and azimuthal angles in MF. For a general polarization, expressed *via* Stokes parameters or other parametrization, or nondipole terms, the full Ω is required.

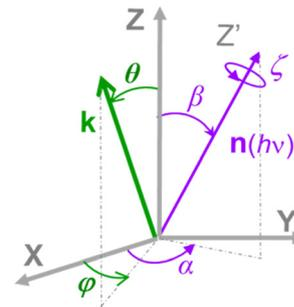


Fig. 1 Schematic of the Euler angles (α, β, ζ) defining the rotation of the molecular frame (X, Y, Z) into the laboratory frame (X', Y', Z') , where the Z' axis lies along the light quantization axis $n(h\nu)$, linear polarization E or propagation axis of elliptically polarized light, and the polar and azimuthal angles (θ, φ) defining the orientation of the photoelectron momentum k in the MF.

Let us consider single photon ionization in the dipole approximation. It is a transition from an initial bound state Ψ_I to a final state characterized asymptotically by an ion in state Ψ_F (with $N - 1$ electrons) and a continuum electron with momentum k , described by a full wavefunction $\Psi_{\text{FK}}^{(-)}$ with appropriate incoming wave boundary conditions. Atomic units (a.u.) will be used.

In MF the differential cross section is given by

$$\frac{d\sigma_{\text{FI}}(\omega)}{dk d\Omega} = 4\pi^2 \alpha \omega \left| \langle \Psi_{\text{FK}}^{(-)} | \hat{E} \cdot d | \Psi_I \rangle \right|^2 \quad (1)$$

here ω is the photon energy, α the fine structure constant, \hat{E} the electric field and d the dipole operator. In the following we shall drop the FI labels relative to the initial and final states. Now one can expand the electron momentum k wavefunction in partial waves as

$$\Psi_k^{(-)} = \sum_{lm} i^{-l} e^{i\sigma_l} Y_{lm}^*(\theta, \varphi) \Psi_{\text{Elm}}^{(-)} \quad (2)$$

where E is the photoelectron energy and Y_{lm} are spherical harmonics. It is convenient to express the dipole in spherical components in LF

$$\hat{E} \cdot d = \hat{E}_\mu d_\mu \quad d_\mu = \sqrt{\frac{4\pi}{3}} r Y_{1\mu}$$

with $\mu = +1, -1$ for left and right CP (LCP, RCP), and $\mu = 0$ for linear polarization. A proper linear combination,⁸ or a photon density matrix⁷ describes the most general polarization.

The dipole is rotated in MF, with a rotation matrix $D_{\gamma\mu}^1$

$$d_{\gamma\mu}^{\text{LF}} = \sum_{\gamma} d_{\gamma\mu}^{\text{MF}} D_{\gamma\mu}^1(\Omega) \quad (3)$$

So, defining the partial wave resolved dipole matrix elements

$$d_{\text{Elm}\gamma}^{(-)} = \langle \Psi_{\text{Elm}}^{(-)} | d_{1\gamma} | \Psi_I \rangle \quad (4)$$

$$d_{k\mu}^{(-)} = \langle \Psi_k^{(-)} | d_{1\mu} | \Psi_I \rangle = \sum_{lm\gamma} i^l e^{-i\sigma_l} Y_{lm}(\theta, \varphi) d_{\text{Elm}\gamma}^{(-)} D_{\gamma\mu}^1(\Omega) \quad (5)$$

In scattering processes, the so-called Wigner time delay is the delay (or advance) that a wavepacket acquires with respect to a



reference (often free evolution) process.⁹ In photoionization if one defines the argument $\eta(E, \theta, \varphi, \Omega)$ of the complex dipole $d_{k\mu}^{(-)}$, the one-photon time delay is expressed by its energy derivative

$$\tau(E, \theta, \varphi, \Omega) = \frac{d\eta}{dE} \quad (6)$$

which in the molecular case depends on the emission angles, molecular orientation and photoelectron energy.^{10–14}

From here, introducing in (1), one arrives at an expression for the differential cross section in MF as a series of angular terms

$$\frac{d\sigma_{\text{FI}}(\omega)}{dk d\Omega} = 4\pi^2\alpha\omega \sum_{LM} A_{LM} Y_{LM}(\theta, \varphi) \quad (7)$$

where the coefficients A_{LM} depend on the orientation and polarization of the radiation field, as well as on the states I, F and on ω . For LP or CP A_{LM} will depend on (β, α) as polar angles, but on full Ω for general polarization. They can be developed in a series of angular basis functions, for instance if light is defined by (β, α) a series of spherical harmonics

$$A_{LM}(\beta, \alpha) = \sum_{JN} A_{LMJN} Y_{JN}(\beta, \alpha) \quad (8)$$

with $J = 0, 1, 2$ limited by photon angular momentum. Both in eqn (7) and (8) real spherical harmonics can be used, as the cross section has to be real.

The coefficients can be analyzed in detail for specific cases, in particular LP and CP cases, linear molecules, core 1s ionizations, other point group symmetries,³ which simplify the full expression, and in particular reduce the number of independent symmetry adapted dipole transition matrix elements. Direct formulas for circular (CDAD) or linear (LDAD) dichroism in photoelectron angular distributions, *i.e.* difference in differential emission probabilities relative to left and right CP or to two perpendicular LP light have been derived.^{6,7} The functions may be directly determined by four independent polarization experiments, and allow to reduce the full MFPAD information, as the cross section dependence on the other angles is expressed through low order trigonometric functions.

An alternative general expression of the MFPAD $I(\theta, \varphi, \Omega)$ was proposed^{15,16} which emphasizes its dependence in terms of low-order trigonometric functions of the electron emission azimuthal angle φ on the one hand, and Ω on the other hand. In the case of single photon ionization of a linear molecule induced by circularly polarized light (CPL), it takes the remarkably simple form

$$\begin{aligned} I_{\pm}(\theta, \varphi, \beta) &= F_{00}(\theta) - 1/2 F_{20}(\theta) P_2^0(\cos \beta) \\ &\quad - 1/2 F_{22}(\theta) P_2^2(\cos \beta) \cos 2\varphi \\ &\quad - 1/2 F_{21}(\theta) P_2^1(\cos \beta) \cos \varphi \pm F_{11}(\theta) P_1^1(\cos \beta) \sin \varphi \end{aligned} \quad (9)$$

Here $\varphi = 0$ corresponds to the plane defined by the molecular and light propagation axes, \pm refers to light helicity and P_L^N are the associated Legendre polynomials. The five one-dimensional F_{LN} functions encapsulate all the dynamical information about

the PI process and are expanded as:

$$F_{LN}(\theta) = \sum_{L'}^{L'_{\text{max}}} C_{L'LN} P_{L'}^N(\cos \theta) \quad (10)$$

where the $C_{L'LN}$ are expressed in terms of the dipole matrix elements¹⁵ and L' runs from 0 up to twice the maximum orbital angular momentum carried away by the photoelectron. It is noteworthy that except for the F_{11} function which is specific to circularly (or elliptically¹⁷) polarized light, the four other F_{LN} functions are identical to those obtained from an experiment with linearly polarized light.¹⁵ Therefore a single measurement using circularly polarized light provides the complete accessible information. CDAD (or LDAD) is expressed simply in terms of the F_{LN} s.¹⁷ The expansion of the MFPAD in eqn (9) is particularly relevant when studying dissociative photoionization of an assembly of randomly oriented molecules with a 4π angle collection of photoelectrons and photoions, and it subtends the extraction of $F_{LN}(\theta)$ functions by performing a (β, φ) Legendre–Fourier analysis of the $I(\theta, \varphi, \Omega)$ measured angular distribution,^{15,16,18} also extended to electron frame EFPADs.¹⁹ It is worth noting that the complete set of emission directions and molecular orientations thereby contributes to the $F_{LN}(\theta)$ determination, obtained with an optimal statistical quality. Eqn (9) (or the related one for linear polarization) then enables to reconstruct specific MFPADs for any polarization geometry at a similar statistical level. This methodology has been applied for several photoionization schemes, involving linear or non-linear molecules of different symmetry, MFPADs and recoil frame RFPADs, one-photon or multi-photon ionization.^{8,20}

Here we stress that the coefficients A_{LM} in eqn (7), or $C_{L'LN}$ in eqn (10), depend on the dipole matrix elements through the products $d_{\text{Elm}\gamma}^{(-)} d_{\text{El}'m'\gamma'}^{(-)*}$. So $d_{\text{Elm}\gamma}^{(-)}$ defined in MF are the basic quantities that connect the wavefunctions to the angular distribution and theoretical calculations to experimental results. From the computed $d_{\text{Elm}\gamma}^{(-)}$ one can derive a theoretical MFPAD, and compare to the experiment, or from the experiment one can derive A_{LM} or equivalent parametrizations, and with sufficient data reconstruct complex dipole matrix elements, up to a so-called complete experiment.^{17,21–24} In principle the (lm) expansion goes to infinity, in practice it converges fast at low kinetic energies. The quadratic nature of the correspondence may give spurious solutions, but generally physical arguments, or even a comparison with theoretical values provides a unique answer. It is also important to remark that the dependence of the A_{LM} on the molecular orientation is linear in a rotation matrix $D_{\gamma\mu}^K(\Omega)$, with $K = 0, 1, 2$ limited by the recoupling of two angular momenta of the photon spin. The so-called polarization averaged (PA) MFPAD,²⁵ corresponding to averaging the MFPAD over all orientations of the radiation, is simply obtained integrating over Ω , which lets surviving the single term relative to $D_{00}^0 = 1$.

If complete orientation is not achieved, averages over the distribution of molecular axes have to be performed. A typical situation occurs in two-body dissociation of polyatomic molecules, giving a so called (recoil frame) RFPAD. Then an average



of the MFPAD around the recoil axis has to be performed.²⁶ If the axis coincides with the MF Z axis, this requires just an integration over (α, ζ) . The RF axis is often assumed to coincide with a molecular bond which breaks, but fast nuclear relaxation may change the direction of recoil. In any case the cylindrical symmetry gives a RFPAD of the same structure as that for a linear molecule.

In general it will be necessary to rotate the MFPAD result to a new reference system before the average, giving

$$Y_{LM}(\theta, \varphi) = \sum_{M'} Y_{LM'}(\theta', \varphi') D_{M'M}^L(\Omega^{-1}) \quad (11)$$

and arrive at

$$\frac{d\sigma_{\text{FI}}(\omega)}{dk'd\Omega} = 4\pi^2\alpha\omega \sum_{LM} A'_{LM} Y_{LM}(\theta', \varphi') \quad (12)$$

Again the coefficients A'_{LM} depend linearly on a rotation matrix D_{PQ}^K . The same logic applies to rotation back of MF to LF. Averages over molecular orientations are now possible.²⁷ In general the molecular orientation in the sample can be described by a distribution function $P(\Omega)$, which we assume normalized $\int P(\Omega)d\Omega = 1$, that can be expressed as a series of rotation matrices, with expansion coefficients (multipole moments)

$$P(\Omega) = \sum_{QRS} C_{QRS} D_{RS}^Q(\Omega) \quad (13)$$

and it is then easy to derive average coefficients

$$\hat{A}_{LM} = \int A'_{LM}(\Omega) P(\Omega) d\Omega \quad (14)$$

Common cases are that $P(\Omega)$ depends only on (α, β) , then $P(\Omega)$ is expressed as a series of spherical harmonics, or a pure cylindrical distribution of Z around Z' (free molecular rotation around Z) with $P(\beta) = \sum_L C_L P_L(\cos \beta)$. In the latter case also the LFPAD will

be a function of the single θ' angle (from now on we shall omit the primes for LF angles, understood from the context)

$$\frac{d\sigma}{d\theta} = \sum_L \hat{A}_L P_L(\cos \theta) = \frac{\sigma}{4\pi} \left[1 + \sum_L \beta_L P_L(\cos \theta) \right] \quad (15)$$

that defines the angular asymmetry parameters commonly denoted by β_n .

Often the distribution $P(\Omega)$ is generated by a laser pulse.^{28,29} For instance, in the most common pump-probe experiment a random molecular sample is excited with a pump pulse to an excited state, whose dynamic will be further followed. In this case the pump generates a molecular alignment with a simple distribution $\cos^2 \chi$ where χ is the angle between the LF polarization axis of the pump and the molecular axis defined by the dipole transition moment of the excitation. Alignment or even orientation with laser pulses has become increasingly effective.³⁰ In particular the creation of rotational wavepackets by tailored pulses generates a time dependent distribution $P(t, \Omega)$ and related $C_{QRS}(t)$ coefficients which induces a time dependent PAD with $\hat{A}_{LM}(t)$ coefficients.³¹ The distribution can be computed by solving the time dependent Schrödinger

equation (TDSE) for a rigid rotor in an appropriate resonant pulse, or can be experimentally characterized, *e.g. via* Coulomb explosion. As the $\hat{A}_{LM}(t)$ depend linearly on the products $d_{\text{Elm}\gamma}^{(-)} d_{\text{Elm}'\gamma'}^{(-)*}$ that gives a large set of data which in principle allow the determination of the dipole matrix elements, with the limitations mentioned.

Finally in the case of completely random orientation the integration over Ω produces the well known result

$$\frac{d\sigma}{d\theta} = \frac{\sigma}{4\pi} [1 + \beta_2 P_2(\cos \theta)]$$

or

$$\frac{d\sigma}{d\theta} = \frac{\sigma}{4\pi} \left[1 + \beta_1 \cos \theta - \frac{1}{2} \beta_2 P_2(\cos \theta) \right] \quad (16)$$

for LP or CP left respectively, with β_1 non zero only for chiral samples.

Generally MFPADS and related averages are sensitive to the nature of the ionized orbital, that is both to its composition in terms of atomic orbitals and to the geometrical structure of the molecule, which makes difficult to disentangle the two contributions. A particularly simple case is for core ionization, where the initial orbital reduces essentially to a single atomic orbital localized on the relevant center (or equivalent centers if more than one chemically equivalent atoms are present). Especially at relatively high kinetic energies (some hundreds of eV) also the final wavefunction becomes simpler, and can be approximated by a single scattering by the neighboring atoms in a multiple scattering approach (*vide infra*). This photoelectron diffraction limit enhances the geometrical content of the PADs and is better suited for geometry determination. Also the use of PA MFPADS has been claimed to enhance geometry determination, as the typically large forward peaks towards neighboring atoms are averaged out, maximizing contrast of the interference fringes. Ideally one would like to invert the photoelectron patterns to get real space images.^{32,33} At very high energies Fourier transforms could be used, and proposals for improvement have been put forward.³⁴ As a matter of fact, these are hardly quantitative, and best results are obtained by trial and error fitting to full wavefunction calculated MFPADS.

When more complex mechanisms are responsible for the ionization, most of the discussion remains unaltered, with the substitution of an appropriate operator in place of the dipole interaction. For the higher multipoles of the radiation they can be just added to $E \cdot d$, in particular the magnetic moment (M1) and electric quadrupole (E2). For randomly oriented molecules the corresponding first order PAD (with LP) has been derived,³⁵ involving two additional parameters, usually denoted as γ and δ ,

$$\frac{d\sigma}{d\theta d\varphi} = \frac{\sigma}{4\pi} [1 + \beta_2 P_2(\cos \theta) + (\delta + \gamma \cos^2(\theta)) \sin \theta \cos \varphi] \quad (17)$$

with related expressions for MFPADS.³⁶

In the case of very high energies it is probably easier to work directly with the full plane wave form of the photon field and compute the transition matrix and the cross section as a function of the k_γ vector of the radiation. The PAD can be



always expressed as a series of spherical harmonics, but the coefficients have to be evaluated separately for each orientation of k_r .

The case of multiphoton ionization (MPI) has recently attracted great interest. While a nonresonant ionization can be treated *via* lowest order perturbation theory (LOPT), much used in the atomic case, the most common situation is resonant, especially REMPI($n + 1$), also because of the high density of states in molecules. The simplest treatment assumes a sequential ionization step from the previously reached excited state, and the PAD can be then described considering the molecular alignment of the excited state, like in the (1 + 1) pump-probe scheme already considered. In any case, for randomly oriented initial system, the PAD will be a series^{28,29}

$$\frac{d\sigma}{d\theta} = \frac{\sigma}{4\pi} \left[1 + \sum_{i=1}^{2n} \beta_i P_i(\cos\theta) \right] \quad (18)$$

where n is the total number of absorbed photons, and odd coefficients appear only for chiral molecules.

A powerful technique, that can deal also with arbitrary complex pulses, which are at the forefront of current research, is the numerical solution of the TDSE for the pulse.^{37–40} At the end T of the pulse, the initial state $\Psi_I(0)$ is transformed into $\Psi_I(T) = U(T,0)\Psi_I(0)$ and the final probability amplitude of observing the final state is given by the scalar product

$$A_k(T) = \langle \Psi_{\text{Fk}}^{(-)} | U(T,0) | \Psi_I \rangle = \langle \Psi_{\text{Fk}}^{(-)} | \Psi_I(T) \rangle \quad (19)$$

That can be converted to a cross section in the case of sufficiently long and weak pulse,^{41,42} or just an ionization probability, also in the nonperturbative regime. Although computationally expensive it is presently a popular approach, with several techniques available for the numerical solution of the TDSE, and will certainly occupy an important place in future research.

We may finally mention Auger decay. It is actually a double (or multiple) electron ionization, which is a large topic outside our present scope. In most situations it is however well described as a two-step process, *i.e.* the decay of an isolated resonance (the core hole state) in the continuum, caused by the interelectronic coulomb term. At this level Auger intensities are obtained by Fermi golden rule, or Wentzel ansatz⁴³

$$T_{\text{JKI}} = 2\pi |\langle \Psi_{\text{Jk}} | H - E | \Psi_I \rangle|^2 \approx 2\pi \left| \left\langle \Psi_{\text{Jk}} \left| \frac{1}{r_{12}} \right| \Psi_I \right\rangle \right|^2 \quad (20)$$

that can be treated like the previous dipole moment amplitude.⁴⁴ Here Ψ_{Jk} is the continuum wavefunction relative to a double ionized state Ψ_J and the Auger continuum electron. The direct photoelectron and Auger electron pair is however entangled, and if both are measured in coincidence their distributions are not independent, as discussed in a formulation including both electrons.^{45,46}

The description of electronic states

The description of electronic states in photoionization involves many-electron bound and continuum states. For the latter an essential ingredient is the calculation of single electron continuum wavefunctions in the nonspherical molecular potential.

The calculation of bound states is a central theme of quantum chemistry,^{47–49} highly developed, and dominated by the treatment of electron correlation, or many-body effects, that is deviations from the predictions based on the mean field Hartree–Fock (HF) approach. Bound states are important *per se*, as initial, intermediate or final ionic states of the system, and for the calculation of transition amplitudes. Moreover they enter in the formulation of the final continuum, together with the photoelectron wavefunction. The reference point is the HF single determinant (configuration) description of the ground state (GS), with optimum orbitals variationally determined (by the self consistent field, SCF procedure). Orbitals are efficiently obtained by basis set expansion, employing a set of functions (atomic orbitals, AOs, mostly built from Gaussian type functions, GTOs) centered on the various atoms. These provide the occupied orbitals as well as a complementary set of excited state molecular orbitals (MOs). From the full set of occupied and excited orbitals, excited configurations can be constructed, and linear combinations (configuration interaction, CI) may be determined by diagonalizing the Hamiltonian, to describe both excited states and introducing correlation. Taking all configurations into account, so called full CI, is prohibitive except for the smallest orbital spaces, and truncations have to be introduced, which strongly affect the quality of the results. The simplest is truncation on the order of excitation, like Singles (S), doubles (D) and so on (T, Q). Going beyond the singles and doubles (SD) excitation level is very expensive, but an accurate choice is to generate SD excitations starting from a selected set of strongly interacting configurations, called multireference CI (MRCI). If in addition orbitals are optimized then multiconfigurational SCF (MCSCF) wavefunctions are obtained, the most common variant being CASSCF (complete active space, *i.e.* full CI over a restricted orbital space) or RASSCF (restricted active space, *i.e.* one or two electrons outside the CAS space). Corrections due to configuration mixing can be obtained by perturbation theory (PT), and often PT is included on top of CI, to correct for the next layer of configurations omitted (MRCI-PT, CAS PT2, RAS PT2).^{50,51} A different expansion based on an excitation operator in exponential form generates the coupled cluster (CC) expansion like CCSD, CC3, which includes products of lower order excitations, *via* nonlinear optimization, satisfying important formal requirements (size extensivity) and a more complete treatment of correlation. A different approach is based on the response (linear, quadratic, *etc.*) of the system to an external perturbation, or to the calculation of propagators (or closely related green functions (GF) or equation of motion (EOM)), which directly approach the excited (ionized) states and the relevant transition amplitudes without explicitly computing excited state wavefunctions. The lowest order approach is random phase approximation (RPA) for excitation. Widely used are OVG (outer valence Greens function)^{52,53} and the algebraic diagrammatic construction (ADC(n)),^{54–56} where n is the order of PT



employed, which has been recently reformulated as a wavefunction approach (note that different formalisms are required for excitation, ionization, *etc.*) and the LR or EOM approaches based on the CC ground state (EOM-CC)⁵⁷ at different excitation levels.^{58,59}

A similar approach is the SAC CI wavefunction, specifically designed for excitation and ionization.⁶⁰ These approaches are very effective for a balanced treatment of correlation, but suffer when a multireference treatment is required. Finally a different theoretical approach is density functional theory (DFT),^{61,62} although most common implementations, based on the Kohn–Sham (KS) approach are formally similar to HF, differing in practice for the HF exchange potential substituted by an exchange–correlation potential V_{XC} , partly theoretically derived, which includes some correlation. In practice DFT works quite well, and in case of local V_{XC} potentials it is also computationally easier. It is difficult however to treat multiconfigurational states. Also fully time dependent DFT equations are computationally viable and often employed. The linear response approximation, TDDFT,⁶³ formally identical to RPA, is widely employed for the treatment of excited states, as well as for continuum calculations.⁶⁴

It must be recognized however that the ability to use a very accurate approach is often restricted to rather small systems because of the computational demands, and that may still represent a limitation in the case of molecules with complex electronic structures where correlation effects play a prominent role, like systems with open shells, excited multiconfigurational states, or with transition metal atoms.^{65,66} Correlation effects appear very clearly in photoelectron spectra by the presence of final states (satellites) relative to multiple electronic excitations, forbidden at the HF level.^{67,68}

The situation is significantly more complex for the final continuum states. The final state has to obey scattering boundary conditions which pose significant problems both for the description of the photoelectron and the structure of the many electron wavefunction. The current strong interest in the description of ionization processes, both in the few photon and strong-field regimes, and the time resolved processes that can be addressed by the ultrashort pulses available with new laser/FEL sources have prompted several groups to propose new algorithms and computer codes.^{69–74}

In principle a very accurate representation of the continuum states can be achieved by the so-called close-coupling form of the wavefunction

$$\Psi_{E\alpha} = \sum_{\alpha'} \Psi_{F'} \phi_{E\alpha'\alpha} + \sum_K C_{EK\alpha} \Phi_K \quad (21)$$

where α includes the index F of target (ionic) states and the rest of labels needed to specify independent continuum channels. It generalizes the CI approach to the continuum states, satisfying the required boundary conditions. It includes a sum over all target states $\Psi_{F'}$, strongly interacting times a corresponding continuum orbital $\phi_{E\alpha'\alpha}$, and a sum over bound state wavefunctions Φ_K to describe short range correlations and possibly autoionizing states, although there is some freedom to move bound state components between the two expansions, and special constraints are needed to ensure a unique solution.

Many specific approximations are possible depending on the type of target states employed and the quality of their description. The single channel (SC) approach limits the expansion to a single term

$$\Psi_{E\alpha} = \Psi_F \phi_{E\alpha} \quad (22)$$

including only the ionic term of interest (thus neglecting interchannel coupling and short range correlations). In this case defining the Dyson orbital as the overlap between the N -particle initial state and $N - 1$ final target

$$\phi_{FI}^D = \sqrt{N!} \int \Psi_F^{N-1*}(x_2, \dots, x_N) \Psi_I^N(x_1, x_2, \dots, x_N) dx_2 \dots dx_N$$

which is readily calculated from the bound wavefunctions Ψ_F and Ψ_I , relative to the ion and the initial state,^{51,58,59,75} the transition dipole moment (4) reduces to a good approximation as a single particle transition moment between the Dyson and the continuum orbitals

$$d_{Elm\gamma}^{(-)} = \left\langle \phi_{Elm}^{(-)} | d_{1\gamma} | \phi_{FI}^D \right\rangle$$

In the simplest approach, with bound states described by single Slater determinants, Dyson orbital reduces to the orbital in the initial state which is ionized, *i.e.* removed in the ionic state. So in the static exchange approximation (SE), the continuum is calculated in the frozen HF potential of the ion, and the dipole transition between the latter and the corresponding HF orbital. In the similar static DFT approach the same procedure is applied with orbitals solutions of a frozen DFT (also called Kohn–Sham) Hamiltonian describing the ground state. These are the most commonly used approximations employed for larger systems, or for large scale calculations. They can be generalized to a linear response theory, which includes interchannel coupling, giving the random phase approximation (RPA) in the *ab initio* framework or time dependent DFT (TDDFT) approaches, the latter more commonly employed in molecules.⁶⁴ It is however easy to include a highly correlated target state, if correlation within the bound states is important. It is also viable to couple *via* Dyson orbital a continuum electron wavefunction separately obtained, at a simpler level, *e.g.* analytical,⁵⁸ or DFT (TDDFT).⁵⁹

In any case the most important issue is the calculation of the continuum orbitals, which lie outside the Hilbert space and are solutions of an (integro)differential equation with appropriate boundary conditions. Simple approximations like plane waves (PW) or Coulomb waves (CW) and orthogonalized variants (OPW, OCW) are often quite poor at low to moderate electron energies, especially for angular distributions. In the atomic case the problem reduces to a set of, possibly coupled, ordinary differential equations (ODE) in the radial variable, that can be efficiently solved by finite difference techniques. In the case of nonspherical molecular potential the situation is more difficult. A one (single) centre expansion (OCE or SCE) can be employed with finite differences, still giving coupled ODEs which are reasonably good for small molecules, but converge very slowly in the case of heavy atoms far from the expansion centre. Alternatively cartesian grids have been employed, especially for



or Multiconfigurational Time Dependent Hartree (MCTDH).⁹⁹ For more details see the companion perspective.¹

Improvements both in algorithms and computer implementations also exploiting hardware development and massive parallelism, is certain to take place, to improve accuracy and increase speed, and make them available to a wider community, like is the present case with highly developed Quantum Chemistry programs for bound states.

In conclusion there is a tight dialogue between theory and experiment. Experiment is a constant challenge to theory, to refine formulations and approximations, both to devise a correct description of novel processes and to push for increased accuracy. Theory helps experiment by building bridges between observables and the underlying structure of the systems studied, by deepening understanding and by providing some missing data.

Experimental methods and tools

In this section we focus on two major directions characterizing the instrumental methods which value angle-resolved studies of molecular photoionization in the laboratory and in the molecular frame, namely the continuous advancement in electron (and ion) momentum imaging spectrometers of large angular acceptance, and the flourishing laser-induced molecular alignment and orientation techniques. At the core of photoelectron science naturally stands the impressive development of advanced light sources, new generations of free electron laser and synchrotron radiation facilities, table-top femtosecond lasers at infrared (IR) and mid-infrared (mid-IR) wavelengths, high-order harmonic generation (HHG) laser based sources of attosecond XUV pulses: their key role and their adequacy for the research projects covering different light-matter interaction regimes and employing different techniques are addressed and referenced in relation with the experiments evoked in this perspective and related publications. Another aspect, underlying the extending field of photoelectron studies towards molecular systems of increasing complexity, is the chemical and physical handling of the samples. While supersonic expansion and seeded molecular beams, continuous or pulsed using mostly an Even-Lavie valve,¹⁰⁰ are central for setting a localized, rotationally cold sample of molecules, a number of challenging issues are at play to bring large molecules *e.g.* organic or biomolecules from liquid or solid to the gas phase, control their quantum state, discriminate isomers, conformers, clusters, *etc.*, involving a variety of sophisticated methods. For these aspects, complementing recent reviews and results,^{101–105} we refer as well to the relevant publications.

Momentum imaging spectrometers

Nowadays, most of the experiments aiming at the measurement of angular distributions of photoelectrons in a broad kinetic energy range (from hundreds of meV to hundreds of eV) rely on efficient momentum imaging spectrometers where charged particles emitted at the crossing of the light beam and the molecular beam are driven from the interaction region towards multi-dimensional position sensitive detectors (PSDs) by electrostatic

fields ensuring a 4π angular collection. Two main approaches form the basis of the flourishing developments observed within the past 30 years, which may be selected according to the targeted scientific needs, and the characteristics of the light sources used. We first describe briefly the main features of electron-ion coincidence 3D momentum spectrometers, referred to under the generic name of reaction microscopes, at the core of many experiments addressing molecular frame or recoil frame photoelectron angular distributions (MFPADs or RFPADs) of diatomic and small polyatomic molecules, now extending to larger molecular systems, of the order of 10 atoms. We then consider devices relying on Velocity Map Imaging mostly used in photoelectron spectroscopy to measure LFPADs for an assembly of randomly oriented molecules, described by a set of β asymmetry parameters, or reaching molecular frame angular features in presence of laser aligned molecules. Both approaches are combined in recent “hybrid” spectrometers or end stations to achieve optimal performance according to the light source and scientific context, as sketched below.

Building on photoelectron-photoion coincidence detection methods (PEPICO),^{106–108} and pioneering measurements of PADs in the molecular frame,^{4,109–111} double particle imaging spectrometers encountered a large development since the late nineties,^{111,112} driven in part by the experimental determination of MFPADs in dissociative photoionization processes. Electron-ion coincidence 3D momentum spectrometers measuring both the impact position (x,y) and the arrival time (t) for each particle arising from photoionization of a single molecule and guided to the relevant electron or ion PSD using uniform electrostatic fields,^{113–115} or parallel electrostatic and magnetic fields in COLTRIMS Target Recoil Ion Momentum Spectroscopy (COLTRIMS) setups,^{116–119} provide event-by-event acquisition of the correlated 3D initial momenta of all emitted charged particles, featuring a kinematically complete description of each ionization event. For dissociative photoionization which prevails for inner-valence and inner-shell ionization of molecules, the measured correlated photoelectron and photoion velocity vectors (or momenta) from initially randomly oriented molecules provide MFPADs when dissociation of the molecular ion is rapid compared to molecular rotation *i.e.* within the axial recoil approximation.^{120,121} As defined in the formalism section, for each DPI process characterized by a set of photoelectron energy and kinetic energy release (KER) of the fragments, the fourfold MFPAD stands here for the (θ,φ) photoemission diagram in the MF, for any orientation (β,γ) of the molecular axis relative to the field frame in the general case of elliptical polarization. PSDs used in these coincidence 3D momentum spectrometers consist of a set of multichannel plates (MCPs) of currently 80 mm or 120 mm (up to 150 mm) diameter and an anode which relies mostly on delay-line fast timing technology.^{122,123} The latter is made of two or three copper coils coupled with a multichannel time-to-digital converter (TDC), providing the impact position and the arrival time for each particle with typically a time precision of 100 ps and a spatial resolution up to 45 μm ,¹²⁴ and few particle multihit capabilities. The ion time-of-flights (TOF) are typically in the range of several microseconds (μs), with backward-forward (BW-FW) extension of few hundreds of



Most recent developments aim to gather the advantages of both approaches, the focus being to create samples of sharply aligned molecules preferentially under field-free conditions. Combining quantum-state selection with specific pulse shaping of the aligning laser pulse has recently demonstrated unprecedented degrees of field-free alignment (1D) for the linear OCS molecule ($\langle \cos^2(\theta_{2D}) \rangle \approx 0.96$,¹⁸⁸ and (3D) for generic asymmetric-top molecules such as indole C_8H_7N with a 3D metric degree ($\langle \cos^2 \delta \rangle \approx 0.89$).¹⁸⁹

Moreover, the limitation of impulsive field-free laser alignment time-windows to about 1 ps within the revivals, demonstrated for small and linear molecules and appropriate for time-resolved investigations using MFPADs as probes of ultra-fast electronic and nuclear dynamics processes, *e.g.* chemical reactions at conical intersection, charge migration, dissociation, fragmentation..., motivates new developments where field-free alignment can last for several ps in the perspective of studying time-resolved molecular dynamics in an extended time-scale.

One recent progress is the design of moderately-long (100 ps) rapidly-truncated (few ps) pulses, where after a slow adiabatic turn-on of the alignment laser pulse up to the peak, realizing optimal alignment, a sharp non-adiabatic cut-off is applied which drops the intensity to less than one per cent using a single passive optics,¹⁹⁰ ensuring high repetition rates and very good contrast. Such spectrally truncated chirped pulses based on a longpass optical filter generating switched wave packets with few rotational states were used to demonstrate field-free alignment of linear (OCS) and asymmetric top molecules such as iodobenzene, with alignment coefficients at the observed revivals close to those reached by adiabatic alignment.¹⁹⁰

Another remarkable achievement is the demonstration of laser-induced 1D¹⁹¹ and 3D¹⁹² alignment of molecules dissolved in He nanodroplets, in both the adiabatic and non-adiabatic limits, which significantly extends the range of applications of structural and dynamical investigations.¹⁹³ This relies on two main properties: on the one hand, the 0.4 K temperature of the He droplets, shared with the embedded molecules, leads to quite high degrees of alignment (0.96); on the other hand, when using sharply truncated laser pulses, the impeding effect of the He environment on molecular rotation increases up to about 10 ps the time-window of field-free strong alignment, occurring right after extinction of the laser field at the peak of the pulse. This powerful technique opens new perspectives for molecular frame experiments, including ultra-fast excited state dynamics, on a variety of large molecules and complexes as demonstrated by 3D alignment of *e.g.* dibromothiophene oligomers¹⁹⁴ or bromobenzene dimers.¹⁶⁵

Finally, we note that all-optical schemes employing intense non-resonant two-color pulses,¹⁹⁵ or based on terahertz pulses,^{196,197} have been proposed to control molecular orientation. A high degree of orientation was recently achieved in *e.g.* OCS with two-color nanosecond pulses,¹⁹⁸ and 3D orientation of polyatomic and asymmetric top molecules demonstrated with two-color femtosecond laser pulses.^{199,200}

Laboratory frame PADs

Photoionization dynamics

The simplest angular distribution in laboratory frame photoionization is that described by the β_2 parameter followed by $\beta_4, \dots, \beta_{2n}$ in the case of multiphoton absorption. It can convey important information on the nature of the target, notably the character of the ionized orbitals. It has been used in the past as a support for the assignment of close-lying ionizations, *e.g.* to distinguish between outer valence σ and π ionizations, or from nonbonding orbitals, in aromatic compounds,^{201,202} where generally π ionizations show a much steeper β_2 increase after threshold. It is clearly sensitive to the AO composition of molecular orbitals. As it depends on the ratios and interference among contributions of different partial waves, it can be more sensitive to some typical continuum structures, like shape resonances or Cooper minima than is found for cross sections. For instance a deep minimum in β_2 at a well defined energy is a clear signature of third row or heavier atoms np orbital participation to the ionized orbital.²⁰³ An interesting case has been recently observed in epichlorohydrine, which presents an outermost composite ionization band, which is found to comprise four ionizations, two of which show a pronounced β_2 well, of different depth, due to Cl 3p AO participation.²⁰⁴ Theoretical calculations employing DFT or HF initial orbitals significantly disagreed with the observed β_2 profiles, and only employing a highly correlated Dyson orbital together with a TDDFT continuum a very satisfactory agreement is reached. This is the first experimental evidence of hole-mixing, or orbital rotation upon ionization, a correlation effect predicted long ago,^{205,206} and typically expected in low symmetry systems with closely spaced ionizations. Recent probes of the orbital character or the role of resonances where emphasized in *e.g.* experimental and theoretical study of β_2 for outer valence ionization of OsO_4 and RuO_4 .²⁰⁷ Also characterization of spin-orbit and ligand field split 4d orbitals ionization in XeF_2 compared with that of Xe was studied.²⁰⁸ A subsequent investigation addressed angular distributions in Auger and resonant Auger from the Xe 3d and F 1s shells.²⁰⁹

Another recent application is in the photodetachment of anions,^{210–213} to characterize the nature of the loosely bound electron, *e.g.* in dipole bound anions. At very low kinetic energies often a single partial wave, s or p, dominates, and is easily recognised by its β_2 behavior. The effect of molecular conformation in a series of substituted phenolate anions was probed through β_2 measurements in different channels, with different sensitivities.²¹⁴ Vibrationally resolved β_2 was observed in the SO_3^- anion, showing unexpected behavior still to be understood. A combined experimental and theoretical study of CN^- close to threshold showed the importance of the contribution of the molecular dipole moment and the improvement over a pure plane wave description.²¹⁵ Effect of correlation and basis set were also investigated.²¹⁶ Not unexpectedly diffuse functions proved essential for a correct description, while DFT orbitals proved close to Dyson ones, but HF significantly worse. The vinylidene–acetylene isomerization was studied through



photodetachment of the H_2CC^- anion,²¹⁷ with characteristic β_2 values splitting into two different groups, reflecting the presence of Franck–Condon forbidden bands activated through vibronic coupling.

Angular resolved PES allows to scrutinize resonances in the ionization continuum of molecules. A study of angular distributions in the two-photon non-resonant ionization in N_2 employing 9.3 eV photons from HHG and a COLTRIMS set-up, measuring β_2 and β_4 , uncovered sharp variations in angular distributions.²¹⁸ The latter have been attributed to dipole forbidden autoionization resonances in the final continuum, supported by an initial theoretical study that treated the ionization as a two step (resonant) process.²¹⁸ Fano resonances with femtosecond lifetime in the same Hopfield continuum were characterized by angle resolved HHG-pump-IR-probe VMI experiments.²¹⁹ Sub-picosecond time-dependent oscillations in the photoelectron yields and angular distributions, and their decay was assigned to interactions within a complex group of resonances close to the $\text{N}_2^+(\text{X})$ ionization threshold at the FERMI FEL.²²⁰ Another example is the determination of the photoemission time delay due to a shape resonance in the $\text{N}_2^+(\text{X})$ state using HHG-second harmonic attosecond stereo-photoionization interferometry.²²¹

Photoelectron spectra are one of the most informative probes of quantum states in pump–probe experiments, *e.g.* studies aimed to disentangle the detailed mechanism of non-adiabatic dynamics in photon induced processes.¹ Often the pure ionization energies (TRPES) are insufficient to unambiguously pinpoint the evolution of electronic states, as they reflect also the changing nuclear geometry. Angular distribution (time resolved PE imaging, TRPEI) may give very valuable information on the nature of the excited states as they are more sensitive to the structure of the relevant orbitals. The ideal goal of fully oriented results is rarely attained,^{222,223} but already β_2 and β_4 are very informative. After some pioneering studies, like excited state dynamics in pyrazine,^{224,225} very few pump–probe experiments include measurements of angular distributions, due to the complexity of the experimental setup. Examples from a study of the dynamics in aniline and some derivatives are reported.²²⁶ A comprehensive discussion of TRPES of pyrazine including calculation of time dependent angular parameters at the DFT level,⁹⁶ is shown to disentangle the contributions due to different channels. It was found that β_4 is very small close to threshold, in agreement with experimental data²²⁷ but increases significantly at higher energies. A clear evolution in such studies has been the development of sufficiently intense sources of higher photon energy. Initial studies employed low photon energy lasers and multiphoton ionization, that were fine for revealing the underlying kinetics, but generally too complex to follow the excited states. An example is the study of acetylacetone dynamics.²²⁸ The development of higher energy laser pulses finally enabled single photon ionization, which is much cleaner to follow and easier to interpret, as in the work on pyrazine.²²⁵ Further developments of FELs, like the seeded Fermi source, allowing the use of still higher energy photons, produce even cleaner photoelectron spectra, avoiding the threshold region, ideally amenable to detailed

theoretical investigations, like that of acetylacetone.²²⁹ Still uncertainties in the nature and the evolution of excited states are present, that cannot be disentangled from the pure photoelectron spectrum. The specific situation in acetylacetone is rather challenging, as the four excited states all involve a single excited orbital, π^* , coupled either singlet or triplet to initial vacancy n (HOMO) or π (HOMO–1), so that ionization always involves the same π^* orbital, and only electron correlation can affect its nature and the relevant photoionization observables. In a recent study of the same dynamics ionized by VUV laser (166 nm) probe²³⁰ β_2 and β_4 were obtained and showed weak but distinct anisotropy, but were not analysed beyond providing independent tests of the timescales. Expanding angular detection in TRPEI experiments is a clear goal for the immediate future.

As mentioned initial multiphoton ionization often provided spectra very difficult to understand. A very large number of studies have flourished thanks to the new experimental facilities available both in the multiphoton and strong field regimes, both employing techniques already available from classical laser studies applied to the new energy domain, and generalizing to new situations possible by the development of precise control over time and phase in multicolor pulses, and structured light. This is a very rapidly developing field, that is not possible to adequately represent in this review, and we shall limit to a few ref. 231–236. Others will be devoted to the special section on chirality and photoelectron circular dichroism (PECD).

Finally LFPADS give additional insights in photoionization studies of more complex species, or targets often problematic to bring in the gas phase. Among these are typically large biomolecules, clusters and nanoparticles,^{237,238} aerosols, and systems at the boundary of condensed phases. Recent activity is on the study of liquids, in particular water and solutions, like droplets or liquid jets,^{239,240} or surfactant layer structure at liquid–vapor interface.²⁴¹

Photoelectron circular dichroism

Photoelectron circular dichroism in single photon ionization of chiral molecules with CP light was theoretically predicted in 1976,²⁴² and realistically calculated by Powis in 2000,^{92,93} which spurred a first experimental confirmation soon after,²⁴³ and a flurry of subsequent work. It consists in a forward–backward asymmetry in photoelectron emission by CP light in randomly oriented molecules, which reverses for different *R* and *S* enantiomers, quantified by the β_1 parameter (sometimes $G = (I_{+1}(0) - I_{-1}(\pi))/I_{\text{tot}} = 2\beta_1$), originating by the mixing of partial waves of different parity. As this is generated by the chiral molecular potential, the effect is quite strong at low KE, but decays fast and is generally negligible after a few tens of eV.

Recent studies detect LFPADS in coincidence with one ionic molecular fragment from a specific dissociation channel, taking advantage of synchrotron radiation extended capabilities (see Experimental Section). This improves the resolving power of the technique, and affords deciphering between different fragmentation channels and/or a specific molecule in a mixture for analytical purposes.¹⁰³ Advances in electron–ion coincidence 3D momentum spectroscopy have allowed full MFPAD experiments,



highlighting for each channel different contributions to the overall measured PECD (*vide infra*).

Furthermore the strong development of laser technology (ns or ps, repetition rate, XUV photon HHG, FELs, strong field) has afforded PECD experiments both in the single photon and multiphoton (especially resonant, REMPI) domains as well as in the strong field regime.^{244,245}

Single photon PECD is now a well established technique that can be used to investigate chemical properties of selected targets. It is essentially a gas-phase technique, due to the ultrahigh vacuum needed to detect electrons, although a first experiment on liquid jets has just appeared.²⁴⁶ In this sense it can be considered complementary to established chiral techniques like CD in absorption, very weak and hard to detect with dilute samples, which is therefore most employed with solutions. Gas phase CD measurements can nevertheless be achieved with special techniques,^{247,248} and have notably been recently demonstrated in mass selected photodetachment of DNA strands.²⁴⁹

While PECD may require special techniques to bring delicate samples in the gas phase, it may probe systems, like anions or cations that cannot survive in solution, or in typical ultrahigh vacuum environments, like the study of surfaces and adsorbates. The absence of solvent interactions also avoids cutoff due to solvent absorption and the process may be easier to simulate theoretically. We shall concentrate on very recent work since many examples are reported in the two most recent reviews.^{102,103} Examples include determination of absolute configuration, molecular conformation, electronic and vibrational structure, and very recent extension to complex biological samples, nanoparticles and liquids. Let us remind that absolute configuration assignment of chiral molecules still presents difficult cases, with relatively few techniques available,²⁵⁰ and PECD stands as a very powerful technique in this respect.²⁵¹

Many details of molecular structure can be analyzed. At variance with IP, σ or β_2 , PECD, like other chiral techniques, is generally very sensitive to molecular conformation, as has been highlighted by theoretical simulations.²⁵² The power of PECD to reveal conformational changes in the gas phase has been highlighted in a study of 1-indanol, where supersonic expansion of the molecule in He and Ar produce a mixture of conformers in the former, but the pure equatorial one in the latter. Despite the superimposable photoelectron spectra and β_2 parameter, PECD showed a clearly distinct behaviour.²⁵³ The conformational dependence is generally hidden as averages in the experimental results, but has been recently investigated in one photon ionization of amino acid proline²⁵⁴ which presents two pairs of stable conformers. It is a rare case where conformers can be discerned by rather different IP's, which allowed to gain detailed information on the dependence of PECD on conformation, as well as of the fragmentation patterns.

A possible link of PECD of amino acids such as alanine and proline with the origin of life's homochirality along with other processes is discussed in the context of astrobiology.²⁵⁵

Another chemically driven investigation is PECD of the organometallic complex Ru(acac)₃ (acac = acetylacetonate).²⁵⁶ It is an example of a class of chiral metal trischelates, of D₃

symmetry. The PES spectrum is very rich, with several well resolved bands, that afford a wealth of experimental data. It proved however very difficult to study theoretically, both for the size of the molecule and the presence of a metal atom, plus the open shell electronic structure which gives rise to multiplets in the PES spectrum, preventing a definite assignment of the spectrum. Actually an older study of the simpler Co(acac)₃, which is closed shell, showed quite satisfactory agreement with theoretical calculations for the HOMO band,²⁵⁷ but very poor for the following ones.²⁵⁸ The problem probably lies in the poor description of ionic states, as is suggested by the bad reproduction of the PES spectrum by the OVG approach, which is generally very accurate for organic molecules. Typically very strong correlation effects appear in transition metal compounds, and PECD can be a powerful tool also for a correct assignment of the spectrum.

The influence of vibrational excitation on the β_1 parameter has been analyzed,⁹⁵ exploiting the large vibrational envelope of the HOMO ionization in 3-carene, which is a rigid molecule, well separated from the following HOMO-1 band. An excellent reproduction of the experimental points by the MS-X α approach is obtained for the mostly adiabatic low energy side of the HOMO band. Scanning the whole band a large variation of β_1 is observed, and comparing measurements along the band at identical electron KE shows conclusively that KE variations are of minor importance for the changes observed. A calculation of FC factors, with harmonic wavefunctions and including Duschinski rotations shows a myriad of vibrationally excited components, overtones and combination bands, although the main peaks visible in the spectrum are associated with the stretching of the C=C double bond, and to a puckering vibration. More insight is obtained by theoretical simulations involving a single vibration at a time. It remains clear however that the overwhelming complexity of the vibrational spectrum precludes a detailed explanation of the observed experimental trends, and call for a full non FC simulation including the majority of the normal modes along with the associated change of the transition dipole moment, still to be developed. A similar study was performed on methyloxirane and the trifluoromethyl derivative.^{259,260}

Investigation of PECD for larger molecules *e.g.* of biological relevance often requires special sample preparation to handle them in the gas phase. Measurements of PECD in photodetachment of amino acid anions²⁶¹ have been performed employing circularly polarized laser beams and electrospray techniques for the preparation of the gas phase samples. Although these are initial results, the potential for the study of complex biological systems is clearly demonstrated. A theoretical simulation on a model anion system by the SCE approach has confirmed the sensitivity of the technique.²⁶² A further extension to the study of PECD in condensed phases, relative to aerosols of the amino acid serine, has been undertaken.²⁶³ Unexpectedly PECD, although reduced in absolute value with respect to the isolated monomer, survives in the nanoparticle, at variance with the β_2 parameter which is totally quenched. Detailed interpretation proves very difficult in such complex systems, and will have probably to rely on phenomenological arguments, but again a



clear indication of the potential of the technique in this area is achieved.

At the more fundamental level is the study of autoionization resonances, effect of molecular orientation, or pump-probe experiments. The behavior of the Fano resonance in β_1 around the first O 1s resonant absorption in methyloxirane was investigated recently.²⁶⁴ While the direct channel is computed to show a negligible β_1 , as expected since β_1 goes quickly to zero at high electron KE, a hundredfold increase due to the interference with the resonance is predicted, with an effect of the order of 2%, which is clearly measurable, and a characteristic dispersion profile across the resonance, in fair agreement with the experimental result. This shows the opportunity of measuring β_1 in resonant Auger spectra, an interesting new possibility. Actually a similar Fano resonance was observed,²⁵⁷ associated with the $3p \rightarrow 3d$ excitation in $\text{Co}(\text{acac})_3$, but at much lower energy, with a typical Fano shape profile.

A two-color pump-probe study involving X-ray femtosecond pulses at the linac coherent light source (LCLS)-XFEL at SLAC National Accelerator Laboratory, the first photon (LP) ionizing a F 1s core in enantiomerically pure trifluoromethyloxirane followed by Auger decay, the second one (CP) probing the PECD temporal evolution for F 1s ionization of the chiral mother-ion in the $(\text{C}_3\text{H}_3\text{F}_2\text{O}^+ - \text{F}^+)$ dissociation channel within few hundreds of fs, was reported recently.²⁶⁵ This experiment, supported by the theoretical prediction of a significant PECD dependence upon the internuclear distance between the ejected F^+ and chiral ionic fragments and the position of the emitter-site, shows the feasibility of XFEL dynamical PECD studies, as a probe of molecular dynamics at distances of the two ions largely exceeding chemical interaction.²⁶⁵

The possibility of employing table top instruments relying on laser technology, even if highly sophisticated presently, is now expanding the availability of the PECD technique to many laboratories. A first experiment producing highly elliptically polarized light from high harmonic generation, has shown the potential to address single photon PECD.²⁶⁶ Most studies have addressed PECD in multiphoton ionization (REMPI). The variety of situations is quite large and we shall limit to a few recent papers, but tracing the first experiments.

More conventional, and practical multiphoton experiments (MP-PECD) carried out few years ago, showed great promise of widespread application, beyond the analysis of higher order processes.^{267–270} Recent developments include the use of a nanosecond laser,²⁷¹ which is found to yield very similar PECD compared to femtosecond, but with large differences in the photoionization rates relative to the intermediate states reached in the $2 + 1$ REMPI ionization subsequent to improved resolution capabilities. This was followed by a high resolution study pinpointing the specific vibronic levels reached through the narrow bandwidth laser.²⁷² A substantial insensitivity of the PECD to the specific vibrational level reached in the resonant excitation was found, which gives confidence in the robustness of the technique for the identification of the molecule and the analytical possibility to identify several compounds in a mixture by selectively tuning to specific resonances. A further study

however showed a more complex situation, suggesting vibronic coupling between close Rydberg intermediate excited states, and a reversal of the PECD for some vibronic state.²⁷³ A similar study has been performed on α -pinene and 3-carene,²⁷⁴ where all individual β_j , up to $j = 6$ have been measured. Those studies highlight the richness, but also the complexity, given the high density of states in the resonant region, of REMPI studies of chirality, and the challenge posed by a detailed interpretation of the results. A recent study illustrated in Fig. 2 employed the same technique to provide detection of absolute configuration in a mixture of chiral molecules, in this case camphor and fenchone.²⁷⁵ By tuning to the 3s intermediate state resonance, which is separated by about 8 nm (114 meV) in the two compounds, almost pure signals from each molecule could be achieved, and PECD was able to differentiate accurately among the four possible enantiomer mixtures, which may become a feasible tool for chiral analysis of mixtures.

Full angular distribution of photoelectrons emitted in $(3 + 1)$ REMPI with elliptically polarized light shows a very complex pattern, with nonlinear dependence on the increasing ellipticity towards CP^{276} associated with the change in molecular orientation distribution reached in the intermediate resonant excitation. From

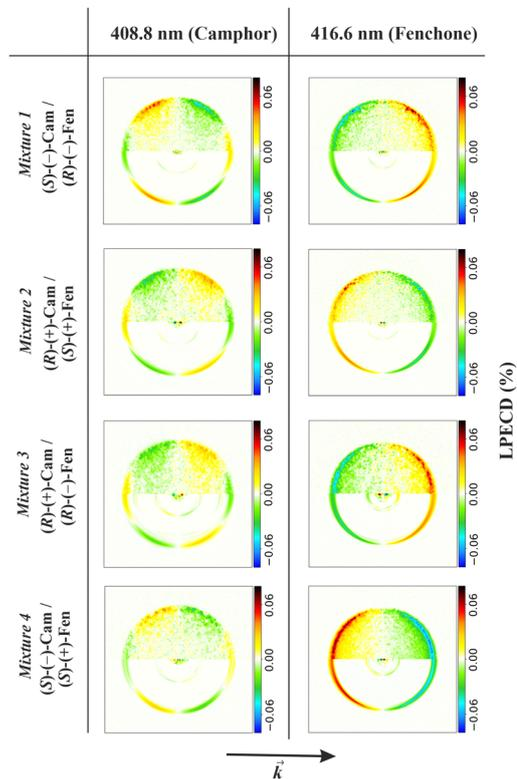


Fig. 2 PECD images extracted from mixtures of camphor and fenchone, relative to the 4 combinations of *R/S* enantiomers, REMPI results relative to excitation at 408.8 nm and 416.6 nm wavelengths, the first resonant for camphor, the second for fenchone.²⁷⁵ Signals from the two molecules can be clearly distinguished, as well as the specific *R/S* combination. Figure reproduced from Fig. 2 of ref. 275 from Physical Chemistry Chemical Physics under Creative Commons Attribution 3.0 International license (<http://creativecommons.org/licenses/by/3.0/>).



molecular frame, presented in the experimental section, *i.e.* (i) working with randomly oriented molecules and determine the effective molecular frame *a posteriori* for each dissociative photoionization event, by means of electron–ion coincidence momentum spectroscopy, or (ii) preparing assemblies of molecules well aligned and/or oriented relative to the field frame, and repeat the measurements for all relevant polarization geometries. Until recently, these two approaches were generally implying different light sources (see Experimental Section): the use of synchrotron radiation facilities well adapted to the conditions of coincidence experiments in therefore weak field conditions, and that of lasers, or free electron lasers, in different field strength regimes, for studies involving aligned targets. However, advancing in the field it is often quite relevant to gather advantages provided by both techniques, which is also supported by the remarkable evolution of the light sources including *e.g.* the increased repetition rate of mid-IR lasers and related XUV HHG sources, and XFELs.

A. MFPADs from randomly oriented molecules: electron–ion coincidence 3D momentum spectroscopy

In single-photon ionization, experiments taking advantage of electron–ion coincidence techniques mostly apply to inner-valence or inner-shell ionization of molecules where the produced cationic states often fragment rapidly, leading to the production of one photoelectron and one or several ionic fragments (if subsequent Auger decay occurs), and for which the validity of the axial recoil approximation can be controlled.^{120,121} Dissociation of the ionic states is either a consequence of steep repulsive potential curves in the Franck Condon region, or, in the case of quasi-bound ionic states due to predissociation subsequent to coupling with a repulsive state. Depending on the associated life-time compared to the rotational period of the cation state, dissociation may be prompt or involve some rotation which must be accounted for in the data analysis. Thus, in the simplest case where a molecular ion dissociates rapidly in two fragments, measuring in coincidence the momentum of the ionic fragment(s) which features the molecular bond at the instant of photoionization, and the ejected electron momentum, provides the photoelectron angular distribution in the molecular frame, for each orientation of the light polarization relative to the molecular axis. Most of the experiments in this section rely on the use of reaction microscopes ensuring a 4π collection angle of electrons and ions as described in the Exp. section.

Here we present selected recent examples illustrating contributions of MFPAD studies to the description of (i) photoionization dynamics, (ii) characterization of molecular structure and dynamics or (iii) fundamental questions in quantum mechanics and light–matter interactions.

Photoionization dynamics

Building on the pioneering expression of MFPADs (Section Formalism)² reflecting the interference of a number of partial waves in the ionization continuum, the goal to access the partial wave resolved complex dipole matrix elements (DMEs), *i.e.* the dynamical

parameters providing a complete description of a photoionization transition from the initial ionized molecular orbital to the ionization continuum for each photon energy was well recognized (see Formalism). It was addressed in the earlier AR-PEPICO studies reported for inner-valence ionization of diatomic and small polyatomic molecules,^{4,110,111,305} and in the first measured MFPADs for K-shell ionization of N_2 .¹⁰⁹ Both inner-valence and inner-shell ionization processes were further on scrutinized in the molecular frame.

Inner-valence photoionization of molecules leads to the production of excited molecular ionic states which involve electronic correlation and play an important role in photochemistry resulting from the interaction of XUV radiation with dilute matter. It gives rise to a number of competing dissociative photoionization (DPI) channels, for which MFPADs stand as fingerprints deciphering the symmetry of the initial neutral ground state and final excited electronic states. Such studies were first carried out for single ionization of linear or small polyatomic molecules using electron–ion coincidence momentum spectroscopy in the axial recoil approximation,^{16,20,113,306,307} although some deviations have also been investigated and exploited to determine a predissociation time or a bending angle in *e.g.* excited states of N_2O^+ .^{308,309} Here we point out briefly some of these results relevant for current studies, most of which were obtained relying on the general description of MFPADs in terms of F_{LN} functions (Section Formalism). An example of the five $F_{LN}(\theta)$ extracted from the measured MFPAD $I(\theta, \varphi, \beta)$ for PI of the NO molecule into the $NO^+(c^3\Pi)$ ionic state induced by circularly polarized light (see eqn (9)) is displayed in Fig. 3(A), together with the result of MCSCI calculations.³¹⁰ Based on the measured F_{LNs} , Fig. 3(B) displays a complete set of four MFPADs featuring the parallel (a) and perpendicular (b) transitions, as well as MFPADs for a molecule oriented at 45° relative to linearly polarized light (c) or at 90° relative to the propagation axis of circularly polarized light (d) which both result from different coherent superposition of parallel and perpendicular transitions.

Magnitudes and signed phases of the partial wave resolved DMEs were determined for selected processes such as PI of the NO molecule into the $NO^+(c^3\Pi)$ state in the region of the $4\sigma \rightarrow k\sigma^*$ shape resonance.^{15,17,23,310,311} The DME dynamical parameters were extracted through a non-linear least-squares fit of the $C_{L/LN}$ coefficients obtained *via* the Legendre polynomial expansion of the measured F_{LN} functions and compared with *ab initio* calculations.¹⁷ A recent highlight illustrating the photoionization dynamics in terms of MF angle resolved photoionization time-delays (see eqn (6)), relying on the derivation of DMEs from measured MFPADs, is presented below.³¹¹ It is noteworthy that the temporal dynamics of this PI process is also addressed in a recent study³¹² relying on the XUV-IR RABBITT (Reconstruction of attosecond beating by two-photon transitions³¹³) interference scheme resolved in the molecular frame.³¹⁴

Another outcome of complete MFPAD measurements is the direct evidence of the CDAD which measures the different MFPAD response of a molecule when exposed to left or right CPL,^{315,316} as predicted and observed in earlier investigations.^{17,317–320} Governed by the F_{11} function in



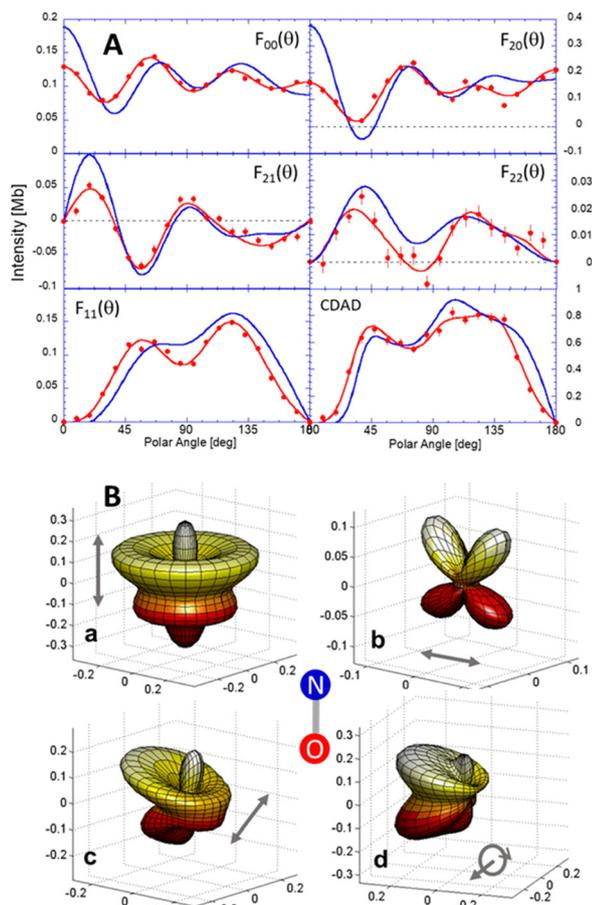


Fig. 3 (A) Measured (red) and computed (blue) F_{LN} functions (see text) and CDAD parameter for ionization of NO into the $\text{NO}^+(c^3\Pi 4\sigma^{-1})$ at $h\nu = 26.35$ eV photon energy,³¹⁰ experiment and theory are normalized such that the total cross-section is identical. (B) Polar and azimuthal dependence of the corresponding measured MFPADs for a linear polarization of the ionizing light parallel (a), perpendicular (b) or tilted at 45° (c) relative to the molecular axis as shown, or for RHC polarized light propagating perpendicular to the molecular axis (d).

eqn (9), the CDAD is a signature of the signed relative phase between the photoionization amplitudes for the parallel and perpendicular transitions, and a sensitive probe of autoionizing resonances.^{316,321} In PI of non-chiral molecules, the CDAD enabled by non-coplanarity of the electron momentum k , the molecular axis and the light propagation axis, quantifies the subsequent right-left anisotropy in the MF described by the azimuthal dependence in $\sin\phi$ in eqn (9). The latter is maximal for electron emission in the polarization plane when the molecular axis is perpendicular to the light propagation axis. It contributes as well to the emission anisotropies observed for chiral molecules as illustrated below, but is distinct from PECD effects.^{322,323}

It is pointed out that when PI is induced by elliptical polarization, the MFPAD general expression encodes the complete polarization state of the ionizing light in terms of *e.g.* the three Stokes parameters.^{17,324} This property has been recently exploited to probe the polarization state of high order harmonics generated

in SF_6 molecules by an elliptically polarized IR field,³²⁵ or driven by intense ultrashort bichromatic circularly polarized fields in Ar.³²⁶

For dissociative ionization of non-linear molecules, the observable consists of the recoil frame photoelectron angular distribution (RFPAD), obtained from the MFPAD by a rotation ($\alpha_R, \beta_R, \gamma_R$) of the MF into the recoil frame (RF) attached to the recoil direction (α_R, β_R) of the ionic fragment, and average of the MFPAD over the azimuthal angle γ_R . For single photon ionization of a molecule of C_{2v} symmetry breaking in two fragments, such as NO_2 where ionization of the ($1a_2$) and ($4a_1$) MOs was studied,²⁶ it was shown that the RFPAD $I(\theta, \phi, \beta)$ takes the same functional form as that of MFPADs for linear molecules, after averaging on the unknown spatial orientation of the molecular fragment, enabling a detailed comparison of measured and computed observables. This method was extended to characterize MPI of *e.g.* NO_2 induced by 400 nm femtosecond pulses, accounting for the partial molecular alignment subsequent to $(n - 1)$ photon absorption.^{133,327}

Structured RFPADs have been reported for single photon ionization of the ($1t_1, 4t_2, 1e$) outer MOs of the CF_4 molecule dissociating into $\text{CF}_3^+ + \text{F}$, for a recoil axis parallel to the polarization.³²⁸ For *e.g.* ($4t_2$) ionization, a striking flip of the RFPAD anisotropy with electron energy is assigned to a strong intra-channel coupling between overlapping shape resonances of a_1 and t_2 symmetry supported by *ab initio* calculations.³²⁸ The PI dynamics underlying the role of these shape resonances is also investigated in two recent time-resolved studies of RFPADs for photoionization of CF_4 , decaying to the ($\text{CF}_3^+ + \text{F}$) channel, using the XUV-IR RABBITT interference scheme.^{329,330}

The latter reveal significant variations of the measured recoil-frame angle-resolved photoionization time delays in the range of a few hundred of attoseconds, in particular asymmetries along the recoil frame axis at the lowest explored energies.³²⁹ The question to which extent the one-photon (XUV) ionization delays can be extracted from the measured MF angle resolved two-photon PI delays is considered.^{329,330} While the single photon ionization delay is well defined and computed as the energy derivative of the phase of the photoionization amplitude (eqn (6)) as illustrated below, that obtained in two-photon XUV/IR RABBITT experiments are more complex to disentangle, as they comprise additional phases, in particular that intrinsically part of the two-photon matrix element involving continuum-continuum transitions.^{10,11,14} In the example outlined here, two theoretical formulations were employed, *via* second order perturbation theory, based on the approximate evaluation of the continuum-continuum transition delay,³²⁹ or *via* a simulation based on the solution of the TDSE with the two colour pulse, which in principle includes exactly all contributions.³³⁰ Both are limited by the treatment of correlation effects, at the Hartree-Fock and Density Functional levels respectively. They show that although following qualitatively the one-photon delays the additional terms are not constant and do not cancel out in taking differences relative to one reference.

For inner-valence ionization of weakly bound systems such as atomic or molecular dimers, an important class of non-local



electronic decay mechanisms is described as Interatomic Coulombic Decay (ICD).^{331,332} In ICD, following ionization of one atom of a dimer, a valence electron fills the vacancy, while the de-excitation energy is transferred to the second atom, causing ionization of a valence electron from that atom. Subsequent Coulomb explosion enables determination of ICD-electron angular distributions in the dimer-fixed frame, as recently illustrated for resonant ICD, following inner-valence Rydberg excitation of $[\text{Ne}^*(2s^{-1}np)\text{Ne}]$ dimers.³³³

Core-shell photoionization of molecules is followed by Auger decay occurring within a few femtoseconds and subsequent Coulomb explosion of the multiply-charged cation leading to the emission of two (or more) ionic fragments, together with the photoelectron and Auger electrons. This provides a vast opportunity for MF characterization of photoionization dynamics of linear and polyatomic molecules, as well as for electronic relaxation and fragmentation dynamics of cationic states. Complete photoionization experiments combining linear and circular (elliptical) polarization states were demonstrated *e.g.* for K-shell ionization of CO and N_2 ,³²⁰ and $(2\sigma_g)$ ionization of N_2 .³³⁴ When using CPL, a large CDAD in the molecular frame was demonstrated for K-shell ionization and identified as a sensitive probe of theory.³²⁰ The photon (or photoelectron) energy dependence of the MFPADs, and that of the magnitude and phases of the DMEs when extracted, provided the orbital angular momentum composition of the electron wave function temporarily trapped in a shape resonance.^{109,334} In this context, K-shell ionization of CO recently led to the extraction of MF angle resolved photoionization time-delays.³³⁵

Molecular frame Auger electron angular distributions (MFAADs) for decay channels stamped by the KER of the ionic fragments allowed to scrutinize the validity of a two-step model, where core-level photoionization and subsequent Auger decay are described as independent steps. While this framework was supported by the dependence of MFAADs on the symmetry of the Auger transition, independent on the orientation of the polarization axis,¹²⁷ small asymmetries of MFPADs correlated with Auger decay channels in *e.g.* C(1s) and O(1s) ionization of CO_2 ,^{336,337} were interpreted as a partial breakdown of the two-step model. MFAADs were shown to disentangle fragmentation pathways of dications, such as symmetric fragmentation, isomerization, or deprotonation in K-shell ionization of acetylene,³³⁸ involving curve crossings and conical intersections, or fragmentation channels subsequent to $1\sigma_g$ and $1\sigma_u$ core ionization of N_2 , resolved by additional coincident angle resolved detection of photoelectrons.^{339,340}

Resonant excitation of a core-shell electron to an antibonding molecular orbital leads to ultrafast dissociation, which may occur on a few femtosecond time-scale comparable to that of Auger decay. There the KER of the fragments encodes the internuclear distance at which ionization occurs, providing an internal clock of the molecular breakup. MFAADs resulting *e.g.* from Cl(2p) excitation of HCl to the 6σ lowest unoccupied MO, corresponding to different KERs, were shown to map the evolution of the ionized orbital from a σ -type MO to an atomic p orbital oriented

perpendicular to the molecular bond,³⁴¹ tracing the electron density temporal evolution during molecular breakup. This strategy is at work in ongoing studies.

With the advent of XFELs, double core hole (DCH) angle resolved Auger electron spectroscopy has emerged as a novel source of information probing the local valence structure of molecules, with first partial MFAADs measured at LCLS on impulsively aligned N_2 molecules.³⁴² Recent experiments characterizing sequential two-photon ionization of O_2 into DCH states based on MFPADs were carried out at the EUXFEL as presented below.³⁴³

For small polyatomic molecules, recording 3D MFPADs is enabled by the coincident detection of the photoelectron with that of three or more ionic fragments subsequent to Auger decay. 3D mapping of photoemission from H_2O was *e.g.* reported measuring 3D momenta of the $(\text{H}^+, \text{O}^+, \text{H}^+)$ ions in coincidence with photoelectron 2D detection, providing MFPADs for the three $a_1 \rightarrow a_1$, $a_1 \rightarrow b_2$, and $a_1 \rightarrow b_1$, ionization channels assigned to well defined polarization geometries, in very good agreement with TDDFT calculations.³⁴⁴ Exploring 3D MFPADs for K-shell ionization of more complex molecules using 3D momentum spectroscopy of both electron and ion fragments is pursued: recent applications address in particular PECD for space-fixed chiral molecules.^{323,345,346}

We illustrate below two recent results addressing MF photoionization time delays, and PAD analysis for core-shell ionization of space fixed chiral molecules.

Molecular frame angle-resolved photoionization delays. In the context of attosecond science, the dynamics of photoionization is often quantified by photoemission delays (eqn (6)). MF angle-resolved attosecond photoionization delays were theoretically predicted for single-photon valence ionization of CO, and N_2 across a shape resonance, for an orientation of the molecule parallel or perpendicular relative to linearly polarized light, highlighting indeed a strong anisotropy of the ionization dynamics.¹³ Angle-resolved two-photon ionization delays in the MF were recently demonstrated using the RABBITT scheme for inner-valence ionization of CO^{314} and NO^{312} molecules, or in the RF of CF_4 as outlined above,^{329,330} which under some conditions can lead to the one-photon quantities.

On the other hand, as outlined above, photoionization delays with complete angular resolution in the molecular frame were recently derived from single-photon MFPADs measured using synchrotron radiation (BESSY and SOLEIL) at a series of spectrally-resolved photon energies across a shape resonance, providing benchmark references for two well characterized prototype reactions, namely K-shell ionization of CO,³³⁵ and inner-valence ionization of $\text{NO}(X^2\Pi)$ into the $\text{NO}^+(\text{c } ^3\Pi 4\sigma^{-1})$ ionic state,³¹¹ and compared with *ab initio* calculations. The magnitudes d_{lm} and relative phases $\tilde{\eta}_{\text{lm}}$ of the partial-wave dipole matrix elements were extracted from the measured MFPADs, providing the complex valued photoionization amplitude and subsequently the time delays for any MF emission direction \hat{k} , or orientation of the molecule $\hat{\Omega}$. The relative phases of the partial wave DMEs were based on a common reference not coupled to the resonance,³¹¹ or deduced from



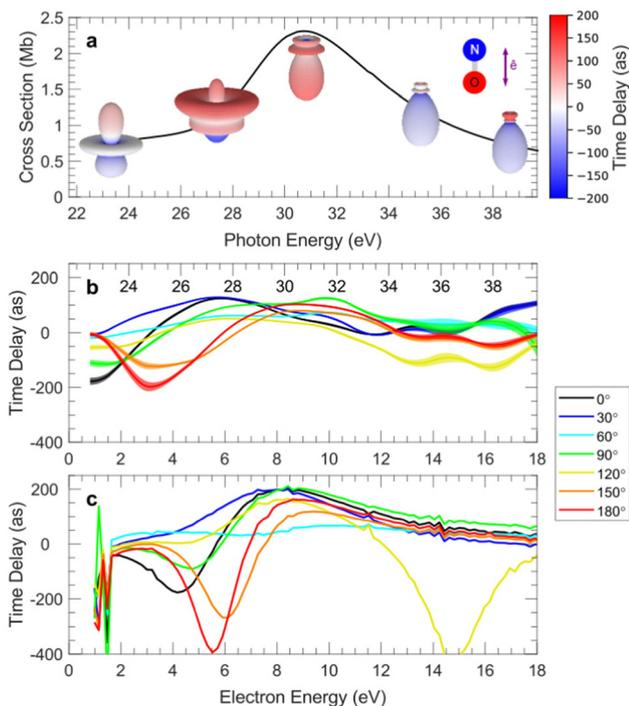


Fig. 4 MFPADs measured at selected photon energies for ionization of NO across the $\text{NO}^+(\text{c}^3\Pi\ 4\sigma^{-1})$ shape resonance, for a molecule oriented parallel to the polarization as shown: the color of the 3D plots features the emission time-delay (a); 1D plots of measured (b) and computed (MCSCI) (c) time-delays, for selected emission angles in the MF.³¹¹

theoretical modelling.³³⁵ MFPADs measured for C(1s) ionization of CO in the range of the first 20 eV above threshold led to the determination of angle-dependent Wigner delays for both ionization into the continua of Σ and Π symmetry, showing evidence of larger delays in the Σ case assigned to the influence of a shape resonance.³³⁵ Results displayed in Fig. 4 correspond to inner-valence ionization of NO in the region of the ($4\sigma \rightarrow k\sigma^*$) shape resonance up to 20 eV above the $\text{NO}^+(\text{c}^3\Pi)$ ionization threshold, as described in Fig. 3 for a given photon energy, selecting an orientation parallel to the polarization axis. Together with the strong variation of MFPADs, the measured and computed photoemission delays varying within a few hundreds of attoseconds reveal comparable strong anisotropies as function of electron energy and MF electron emission polar angle. The observed angular dependence of the MF-resolved time delays is interpreted as a signature of the interference between the resonant and non-resonant components of the photoionization amplitude described by a multichannel Fano formalism, where the ionization delay of the resonant component is angle-independent.³¹¹ These results are coherent with those extracted from measured two-photon delays reported recently for the same reaction.³¹²

Core-shell photoionization of spaced fixed complex molecules: unravelling the building-up of PECD in chiral molecules. O(1s) ionization of uniaxially oriented methyloxirane ($\text{C}_3\text{H}_6\text{O}$),³²³ considered as a showcase chiral molecule in PECD studies, was investigated combining the COLTRIMS-technique

with CPL at SOLEIL, then extended to trifluoromethyloxirane,³⁴⁵ where the CH_3 group is substituted by CF_3 . Selecting equivalent “complete” doubly charged breakup channels, where the momenta of *e.g.* the $\text{C}_2\text{H}_2\text{O}^+$ and CH_3^+ (or CF_3^+) recoil ionic fragments and the photoelectron are measured in coincidence, provided differential PECD (θ_L, β) 2D maps, where the polar angles θ_L and β define the electron emission direction and the molecular orientation relative to the light propagation axis. Quite similar for the corresponding enantiomers of methyloxirane and trifluoromethyloxirane, they demonstrate a strongly enhanced PECD (up to a factor 5) for given (θ_L, β) spots compared to the maximum values measured for randomly oriented targets, generally well described by single center calculations.^{323,345} For a molecular orientation perpendicular to the light propagation direction ($\beta = 90^\circ$) and electron emission in the polarization plane ($\theta_L = 90^\circ$), one obtains the CDAD parameter introduced earlier, which indeed does not contribute to the PECD.

Selecting further *e.g.* a three fragment breakup channel such as $\text{CH}_2^+ - \text{C}_2\text{H}_{2,3}^+$ and $\text{OH}_{1,2}$, after O(1s) ionization of methyloxirane, fixes the molecular frame (close to the fragment recoil frame) in three spatial dimensions, and gives access to MFPADs for each orientation of the light propagation axis relative to the molecular frame.³⁴⁷ These fourfold differential angular distributions, where both the electron emission direction and the propagation axis are defined by a set of polar and azimuthal angles (θ, φ) in the MF, measured for both helicities and enantiomers, can then be interpreted in terms of a PECD(θ, φ) parameter for each orientation of the molecule relative to the light propagation axis, revealing maximum values larger than 50%. A similar analysis in the trifluoromethyloxirane has been further conducted for four initial ionization bands, the two unresolved carbon atoms of the ring, the CF_3 carbon, and the three unresolved fluorine atoms, in addition to oxygen.³⁴⁶ The PECD of space fixed oriented chiral molecules may then stand as a sensitive structural and analytical technique for the enantiomeric excess determination, at the cost however of a more complex experiment. Rationalizing the influence of spatial alignment of molecules photoionized by CPL is as well relevant for the interpretation of PECD studies relying on REMPI which induces partial alignment of the molecule.²³¹ It also supports the interpretation of the strong fragmentation channel dependence of PECD in strong field ionization of methyloxirane³⁴⁸ as attributed to the selection of specific molecular orientations for each fragmentation channel.

On top of the description of photoionization dynamics, core-level ionization 3D MFPAD (or RFPAD) studies have focused on imaging the molecular structure in three dimensions, relying on the localized character of the emission source, spotlighting different perspectives depending on the photoelectron energy.

Molecular structure: photoelectron “diffraction from within”

For carbon K-shell ionization of polyatomic molecules such as methane,³⁴⁹ ethane, carbon tetrafluoride or difluoroethylene,³⁵⁰ 3D MFPADs measured few eV above threshold at the Advanced Light Source (ALS, Lawrence Berkeley National Laboratory) by 3D momentum spectroscopy of both electron and ion fragments with a COLTRIMS end station, revealed that



the maxima in the 3D emission pattern point either along the directions of the molecular bonds (CH_4 , C_2H_6), or away from (bisecting) these directions (CF_4). This striking observation, well predicted by *ab initio* complex Kohn variational calculations, was emphasized when considering polarization averaged MFPADs (PA-MFPADs),^{25,349,350} *i.e.* MFPADs averaged with respect to the light polarization direction, providing a direct imaging of the molecular geometry, or its “opposite”. The generality of these statements has been examined in a theoretical study considering molecules with different atomic centers and symmetries, in an extended electron energy range, where the propensity for direct imaging of molecular geometry by means of K-shell PA-MFPADs was only observed for simple hydrides at very low or selected high kinetic energies.³⁵¹ Still, it was found that this observable can be informative on the three-dimensional arrangement of the system in correlating the anisotropies in PA-MFPADs with partial accumulation of the electron density in the region surrounded by the peripheral atoms. Other investigations fostering quantitative information extractable from PA-MFPADs (or PA-RFPADs), measured using electron-ion 3D momentum spectroscopy at Spring 8, have been reported probing *e.g.* molecular bond-length in O(1s) ionization of CO_2 and C(1s) ionization of CH_3I , relying on the F_{LN} description of MF and RFPADs.^{352,353} The results obtained at different electron energies compare well with MCSCI or TDDFT calculations, respectively, which shed light on diffraction features predicted at higher energies. The interpretation of such PA core-level MFPADs focusing on molecular structure is supported by a full-potential multiple scattering theory for photoelectron energies in the 100 eV range.^{354,355} Further comparative studies of 3D MFPADs measured for *e.g.* O(1s) ionization of methanol with SC calculations,³⁵⁶ and with earlier results for carbon monoxide MFPADs for similar polarization geometries of the CO central bond,¹¹⁸ elucidate the influence of both bond lengths and presence of H additional atoms.

Along with scattering and diffraction of X rays and electrons providing well identified tools for exploration of the structure and properties of matter, it was suggested about two decades ago that MFPADs for site and element specific inner-shell ionization may be interpreted as X-ray photoelectron diffraction (XPD) mapping.³⁵⁷ This representation is supported by the multiple scattering picture of the ionization process, where the emission intensity in a given direction in the molecular frame results from the coherent superposition of a direct wave arising from the K shell of the ionized atom, with those scattered one or more times from the other atoms in the molecule (see Section Formalism). Noting that an electron energy of 150 eV corresponds to a de Broglie wavelength of 1 Å, it is expected that MFPADs including different polarization geometries constitute thereby unique fingerprints of the molecular potential, increasingly informative on the geometry of the molecule for photon energies far from the ionization threshold, supporting the concept of “electron diffraction from within”. This concept supports *e.g.* the interpretation of recent studies aiming at imaging of a molecular breakup using an XFEL illustrated below, and further examples are discussed later in the different contexts of Femtosecond photoelectron

diffraction, and Laser Induced Electron Diffraction (LIED) giving rise to another type of “scattering from within”.

Fundamental studies of light–matter interactions

Fundamental questions in light–matter interactions addressed in the last two decades, relying on coincidence techniques and subsequent characterization of MFPADs, unveiled new quantum phenomena at the molecular scale as illustrated by few examples such as interferences in molecular double-slit or multislit arrangements.^{358–360} Symmetry breaking in resonant one-photon dissociative ionization of H_2 through doubly excited states auto-ionizing on a few femtosecond time scale comparable to the dissociation time was demonstrated through the anisotropies of MFPADs induced by linearly³⁶¹ and circularly³¹⁶ polarized EUV photons, reflecting interferences between channels involving ionic states of different u and g symmetry subsequent to autoionization. Through their fundamental quantum nature, these questions overlap with that of the localized or non-localized character of single-holes in transient short-lived electronic states formed by one-photon K-shell ionization of symmetric molecules with two chemically equivalent atoms. The quantum entanglement of the photoelectron-Auger electron pair in K-shell ionization of N_2 was unveiled by the correlation between MFPADs and MFAADs.³³⁹ Core-hole localization was further characterized by MFPAD or RFPAD asymmetries in K-shell ionization of polyatomic molecules *e.g.* O(1s) CO_2 or F(1s) CF_4 .^{337,362} In S(1s) ionization of CS_2 the localized/delocalized character of the S(1s) hole in the (SCS)⁴⁺ cationic intermediate states formed after Auger decay, was observed in measured and computed MFPADs for selected KERs in the $\text{S}^+ + \text{C}^+ + \text{S}^{2+}$ DPI channel, featuring different relaxation pathways.³⁶³ Another twist of symmetry *versus* localization/delocalization occurs in presence of double well molecular potentials, as featured by a recent theoretical study of angularly and vibrationally resolved valence photoionization of NH_3 , involving the umbrella inversion mode.³⁶⁴ For linearly polarized light parallel to the C_3 symmetry axis, MFPADs show a quite distinct behavior according to the even/odd symmetry of the initial vibrational wavefunction and their incoherent or coherent superposition.

At high electron kinetic energies the continuum wavefunction becomes close to a plane wave, and the transition dipole moment from an initial bound state targeted by a given MO proportional to its Fourier transform. In an experiment on H_2 at 400 eV photon energy with CP light propagating perpendicular to the molecular axis, MFPADs in the polarization plane were measured for the final $1\sigma_g$ ground state of H_2^+ , as well as for the $1\sigma_u$ and $2\sigma_g$ excited states (satellites) resolved *via* the measured kinetic energy release KER of the reaction.³⁶⁵ As the latter ionic states are fully dissociative, the measured KER also led to MFPADs for different internuclear distances within the Franck–Condon region. MFPADs assigned to each excited ionic state provide an image of the corresponding component of the correlated initial state of H_2 . Actually they feature an image of the Dyson orbitals relative to the corresponding final states of H_2^+ . This work of general application highlights the interest in measuring MFPADs of



satellite states, which convey important information on the electronic correlation within the neutral molecule.³⁶⁶

Building on the remarkable developments of advanced light sources based on third generation synchrotron radiation, free electron lasers and lasers, more extreme regimes of the light-matter interaction are being explored accessing new ionization mechanisms and dynamics.

Non-dipole and recoil effects. Reaching the hard X-ray regime in photoionization,²⁹⁵ significant non-dipole effects, as well as consequences of the recoil imparted to the nuclei by the fast photoelectron and high energy photons, are expected to translate into MF photoemission properties. This energy domain has specific implications for molecular dynamics with recoil induced vibrational and rotational excitation,³⁶⁷ or for post collisional interaction (PCI) effects between a slow photoelectron and a fast Auger electron. The latter were shown to have an increasing influence on angular momentum distributions in K-shell ionization of atoms,³⁶⁸ to be further explored in molecules.

In the follow-up of LF characterization of non-dipole and recoil effects outlined earlier, full MFPADS were measured for $N_2(1s)$ ionized with an excitation energy of 40 keV through the coincident detection of two N^+ fragments and one Auger electron, the fast photoelectron momentum being deduced by momentum conservation, and compared with SCE calculations.³⁶⁹ A remarkable two-fold emission anisotropy is observed in the MF. On the one hand a forward-backward asymmetry with respect to the photon momentum, favoring FW emission, is found for any orientation of the molecular axis, resulting in the anisotropy measured in the LF, well predicted at the MF level by theoretical calculations including the full photon plane wave $e^{ik \cdot r}$. On the other hand, an additional MFPAD strong asymmetry along the light polarization axis is noted when the molecular axis is neither parallel nor perpendicular to the photon momentum (or the polarization axis), favoring emission in the direction of the FW nitrogen atom: in the calculations a very weak dependence of the MFPADs relative to the molecular axis alignment was obtained, unless the combined impact of the sum of the recoil momentum of the fast photoelectron and the linear momentum of the high energy photon on the nuclei was properly taken into account, leading to a very good description of the newly observed symmetry breaking of MFPADs relative to the light polarization axis. Such effects will influence the interpretation of high energy experiments scheduled at XFELs.

Another manifestation of nondipole effects was highlighted in a recent study aimed at quantifying the time delay relative to photoionization by different parts of an extended molecular orbital.³⁷⁰ The experiment considered double ionization of H_2 by 800 eV photons with coincident measurement of the momenta of the H^+ ions and the slow photoelectron, providing MFPADs of the fast photoelectron, in conditions where double-slit interference effects are met and the MFPADs are analyzed as fringe patterns. Recording the position of the fringes as a function of the light propagation direction with respect to the molecular axis, a displacement of the fringe pattern is observed, which is maximal when both axes coincide. This

phase shift of the photoionization amplitude is assigned to a variation of the electron birth time delay and can be interpreted as the time the light takes to move from one proton to the other, that is estimated as 247 zeptoseconds, coherent with the average internuclear distance and the velocity of light.

This result can be clearly interpreted as a non-dipole effect, which takes into account the spatial variation of the field, neglected in the dipole approximation. It generated a flurry of theoretical work, employing a real time dependent description through TDSE, which included retardation in the field description.^{371–373} An alternative approach, based on the use of a high intensity 100 eV pulse, has been studied theoretically solving the TDSE including first-order nondipole effects, and interpreting the results *via* a simplified analytic model, showing the ability to detect the expected sub-as delays.³⁷⁴

Multiphoton processes in the X-ray regime have been explored theoretically, *e.g.* Stimulated Compton scattering (SCS).³⁷⁵ Significant asymmetries in the MFPADS of the low energy electrons are calculated, which also depend on the orientations of both light propagation and polarization directions in the MF.

Photoionization in intense X-ray femtosecond pulses at XFELs. Illustrating the opportunities raised by the advent of XFELs delivering femtosecond pulses of high intensity, with increasing repetition rate which opens the road to the implementation of multiparticle coincidence experiments, recent results demonstrate two-photon K-shell sequential ionization of O_2 and the subsequent temporal break-up of the ionized molecule at the European XFEL,¹⁴³ using a COLTRIMS reaction microscope end station permanently installed at the Small Quantum Systems (SQS)

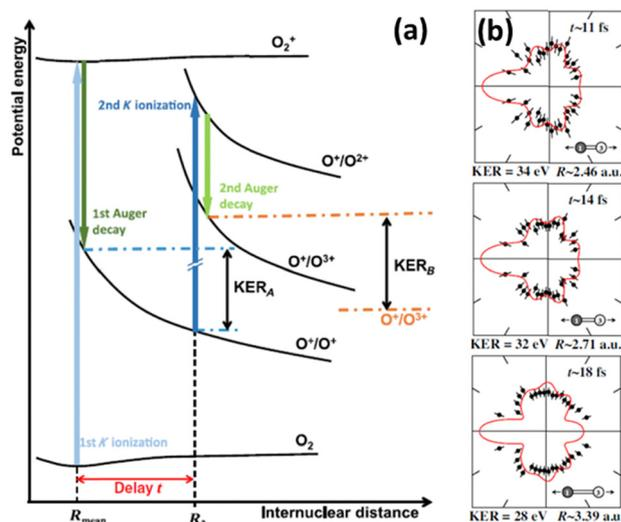


Fig. 5 Schematic of the PAP two-photon K-shell ionization of O_2 leading to the $(O^+ + O^{3+})$ channel³⁷⁷ based on typical potential energy curves, featuring the internuclear distance R_2 and delay t for the second photon absorption (a); measured (dots) and computed (red line) PA-MFPADs for three KERs assigned to (R,t) parameters, assuming a second photon absorption by the K orbital of the right-hand O ion (labeled "3" in the inset) (b). Figure adapted from Fig. 2 and Fig. 6 of ref. 377 with permission from Physical Review X under Creative Commons Attribution 4.0 International license (<http://creativecommons.org/licenses/by/4.0/>).



beamline.³⁷⁶ Recording ion–ion–electron coincidence momenta at a photon energy of 670 eV, *i.e.* 127 eV above the O(1s) threshold, MFPADs featuring emission of the second photoelectron were measured and assigned to two different ionization schemes.³⁴³ In the first sequence described as photoelectron–Auger electron–photoelectron (PAP),³⁷⁷ leading *e.g.* to the ($O^+ + O^{3+}$) channel after ejection of a second Auger electron, polarization averaged PA-MFPADs sorted as a function of the ion fragment kinetic energy release (KER), asymmetric along the $O^+–O^{3+}$ internuclear axis, display resolved angular lobes as shown in Fig. 5.

Supported by theoretical modeling using the single center method within the relaxed-core Hartree–Fock approximation, these MFPADs are interpreted as photoelectron diffraction patterns imaging the increase of the internuclear distance during the X-ray induced breakup of the O_2 molecule. Thereby the internuclear distances and times where the second photon is absorbed within the 25 fs pulse can be inferred, revealing a first molecular movie of sequential core–hole ionization.³⁷⁷ The experimental and computed angular distributions in qualitative agreement support the feasibility of making molecular movies using upcoming two–pulse pump–probe schemes at high repetition rate XFELs. On the other hand, inspection of the coincidence maps correlating electron energies, or the ion fragment KER and electron energy, for ($O^{2+} + O^{2+}$) channels, demonstrates the generation of double core–hole (DCH) ionic states,³⁴³ produced in an ionization sequence where ultrafast ejection of the two photoelectrons, occurring typically within less than 5 fs, precedes Auger decay. These energy maps allow to identify single-site (SS) and two-site (TS) DCH states, corresponding to emission of the two K-shell electrons from the same atom, or from different atoms. MFPADs for these processes have been obtained for the first time and constitute sensitive probes of the inherently different charge distribution of both channels.

Strong field tunnel ionization. Ionization of molecules in intense laser fields is a fundamental process which governs a number of strong field phenomena, such as high-harmonic generation, or laser induced electron diffraction. Although SFI studies mostly rely on experiments involving laser molecular alignment (see section: MFPADs from laser aligned molecules), significant results have been reported using randomly oriented molecules.

MF photoemission resulting from tunneling ionization of randomly oriented H_2 ,³⁷⁸ or HCl ³⁷⁹ molecules was studied using a COLTRIMS set-up and an intense femtosecond IR circularly polarized laser (10^{14} W cm^{-2} , 40 fs 800 nm) with the intent to image electronic structure fingerprints. In this case, although the highest occupied molecular orbital (HOMO) is primarily ionized populating bound ionic states, dissociative ionization occurs due to bond softening and their coupling with a higher dissociative state, providing access to correlated electron and ion fragment momenta detected about the polarization plane. The anisotropy of the subsequent MFPADs highlighted a favored tunnel ionization parallel to the molecular axis of H_2 , and the effective participation of the HOMO–1 lower valence MO in tunneling from HCl , reflecting many-electron effects and the formation of a correlated ion. For HCl , the

observed asymmetry of the ionization probability along the molecular axis can be assigned to the dipole moment of the molecule. Such observables have stimulated theoretical modelling of strong field ionization in molecules.

Combining angular streaking with electron–ion coincidence 3D momentum spectroscopy of strong field multielectron dynamics is further illustrated in recent experiments carried out using 3D coincidence VMIs.¹⁶² RFPADs measured in the polarization plane of intense circularly polarized IR femtosecond pulses for dissociative ionization of polyatomic molecules such as methyl iodide CH_3I were reported for single and double ionization featuring as well angle-dependent ionization yields reflecting contributions of both HOMO and HOMO–1 orbitals.³⁸⁰

Beyond setting electron tunneling as a tool for imaging the electronic structure of single molecules, further research investigates the detailed dynamics of tunnel ionization and its characterization by Wigner time-delays τ_w , defined as the energy derivative of the phase of the electron's wavefunction in momentum space. Most recent results address the dependence of $\tau_w(E, \beta)$ Wigner delays on the electron energy and emission angle β with respect to the molecular axis, here H_2 , within the polarization plane of circularly polarized laser light.³⁸¹ To access the phase information carried by the detected electron wavepacket, an interferometric method termed holographic angular streaking of electrons (HASE) has been developed,³⁸² where ionization is triggered by a co-rotating two-color ($2\omega, \omega$) laser field, formed by superposition of two circularly polarized femtosecond laser pulses. The observed Wigner time delays, extracted from the MFPADs obtained using a COLTRIMS reaction microscope, are assigned to spatial shifts of the electron birth positions when emerging from the potential barrier.

B. MFPADs from laser aligned molecules

Other strategies to measure MFPADs are dictated by the different means to establish the molecular frame experimentally, or by extracting the relevant MF information from LFPAD experiments controlling the rotational degree of freedom in simple molecules. Mostly relevant for photoionization studies of non-dissociative processes, of complex molecules, or using light sources operating at low repetition rates (<1 kHz) unfavorable for coincidence techniques, molecular frame photoelectron angular distributions can be obtained from samples of aligned molecules.

Building on the study of rotationally state-resolved LFPADs for resonance-enhanced two-photon ionization by linearly and circularly polarized light, featured by the $NO A^2\Sigma^+(v, N) \rightarrow NO^+ X^1\Sigma^+(v', N') + e(l, \lambda)$ transition,²¹ providing a complete description of the PI reaction and a demonstration of MF circular dichroism,^{383,384} REMPI of isotropically distributed gas-phase molecules represents one direction to bridge the gap between the LF and the MF.²⁷ It has been extended to characterize the valence PI dynamics of light polyatomic molecules such as acetylene³⁸⁵ or ammonia³⁸⁶ carried into a partially aligned electronic state by the absorption of n pump photons, and ionized close to the ionization threshold by m probe photons, taking advantage of different polarization geometries.²⁹ While the achievable alignment increases with the number of photons involved in the



excitation process, the degree of alignment established for ionization of those excited molecular states remains limited requesting an extensive data processing, and as a purely optical scheme it does not allow for selection of molecular orientation.

Alternative techniques rely on laser induced molecular alignment and orientation. Whether one considers adiabatic or nonadiabatic laser molecular alignment (see Exp. section), setting a photoionization experiment from aligned molecules requires a pump–probe scheme where the alignment laser and the ionizing “probe” laser pulses are temporally resolved. The latter may consist of an XUV femtosecond pulse, *e.g.* produced by HHG leading to single photon ionization in weak field conditions (perturbative regime) or by free electron lasers (FEL) for which high fluxes allow for multiphoton processes still in the perturbative regime, a pico-to-femtosecond UV pulse initiating a REMPI process (perturbative multiphoton), or an IR or mid-IR intense laser involving strong field ionization. All these situations are indeed met and exploited in the ongoing research as briefly sketched in this section. The dependence of ionization yields measured at aligned or anti-aligned revivals, with reduced information with respect to MFPADS but still quite informative, remains attractive with the advantage of a simpler experimental setup: it was *e.g.* recently used at FERMI, combined with photoelectron spectra, as a control variable of the dissociation pattern for single photon inner-valence ionization of acetylene in the XUV photon energy range.³⁸⁷ It serves as well as a probe of strong field ionization as outlined below.

First demonstrations of MFPADS measured from impulsively aligned molecules were achieved in femtosecond time-resolved studies, where photoionization acted as a probe of electronic–vibrational dynamics in photodissociation of CS₂ excited states.^{222,223}

Valence-shell ionization of aligned molecules

MF photoemission for valence-shell ionization of CO₂, N₂, O₂, CO molecules into bound ionic states was highlighted in the last decade combining impulsive alignment by a moderately strong femto-second laser and ionization by an HHG XUV source.^{388–390} Photoelectron momentum distributions recorded with a VMI in field-free conditions, around aligned and anti-aligned revivals of a rotational wavepacket, provided MFPADS for ionization of HOMO, HOMO–1, up to HOMO–4 molecular orbitals, resolved within congested energy spectra in an extended photoelectron energy range (0–30 eV). Different polarization geometries led to MFPADS for parallel and perpendicular transitions (averaged on the MF azimuthal emission angle). The latter, well predicted by MCSCF^{388,389} and multi-channel *R*-matrix³⁹⁰ calculations imprint information on the electronic structure of valence MOs.

PADs for valence ionization of excited states of naphthalene and aniline polyatomic molecules, 1D or 3D adiabatically aligned with 100 ps IR laser temporally truncated pulses, were reported recently for various polarization geometries, in a two-photon resonant scheme using low intensity UV ionizing pulses of few ps duration.¹⁸⁴ For both molecules, the two-photon process is resonant at the one-photon level with the S1 electronically excited state. For the naphthalene molecule, the structured

PADs recorded with a VMI set-up displayed in Fig. 6 show an enhanced anisotropy in presence of the alignment laser. They compare well with numerical simulations of the 2D PADs based on ePolyScat *ab initio* calculations of MFPADS for ionization of the S1 state (averaged on the MF azimuthal emission angle), demonstrating also that a high degree of alignment was achieved. The situation is however different for aniline, which points to the contribution of additional ionization channels, subsequent to the perturbing presence of the alignment laser. This flaw can be avoided to achieve MFPADS for the electronic ground state using VUV single-photon ionization. More generally, these results support the use of field-free molecular alignment relying on the recent achievements (see Exp. section) combining spectrally truncated chirped laser pulses,¹⁹⁰ and long-lasting field-free alignment of molecules imbedded in He nanodroplets.¹⁹⁴ Although imaging of photoions resulting from Coulomb explosion is currently used to characterize their degree of alignment,^{165,194,391} work is still in progress to demonstrate PADs for molecules in He droplets.

Molecular frame reconstruction using time-domain photoionization interferometry

The complete retrieval of dynamical dipole matrix elements by time-resolved TRPADs measurements in LF was demonstrated

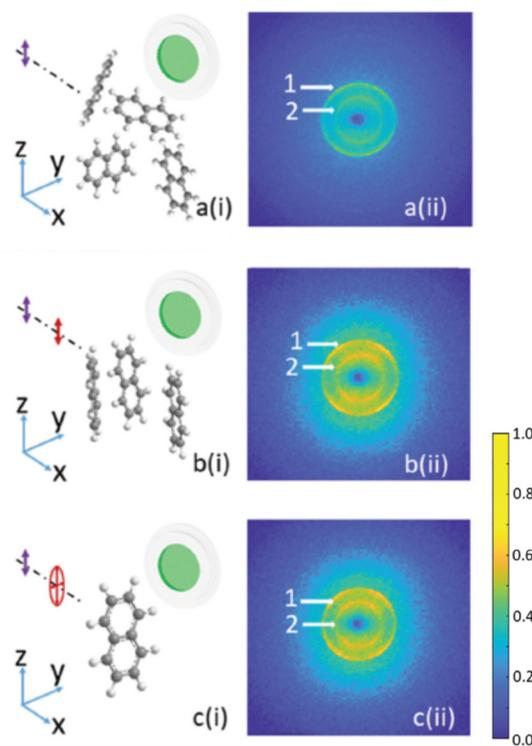


Fig. 6 Photoelectron VMI raw images for two-photon linearly polarized REMPI (293.53 nm) of naphthalene (vertical purple arrow) for: an isotropic distribution of molecules (a), a linearly polarized alignment pulse (red arrow) providing 1D alignment (b), an elliptically polarized alignment pulse (red ellipse) providing 3D alignment of naphthalene.¹⁸⁴ Reprinted with permission by Taylor and Francis, <http://www.tandfonline.com>, from J. Artl *et al.*, Photoelectron angular distributions from resonant two-photon ionisation of adiabatically aligned naphthalene and aniline molecules, *Molecular Physics*, 2021, **119**, e1836411.¹⁸⁴



in $(1 + 1')$ two-photon ionization of rotationally cold NO *via* the $\text{NO}(A^2\Sigma^+)$ state, using a pump–probe scheme based on femto-second UV lasers with variable wavelength of the probe corresponding to 0–1.33 eV photoelectron kinetic energy.³⁹² The observables consisting of (t, E) time-energy maps of LFPADs are described by the time dependent $\beta_2(t)$ and $\beta_4(t)$ asymmetry parameters (together with the cross section), which expand for each energy in terms of the dynamical parameters C_{KQ}^{LM} and the $A_{KQ}(t)$ moments characterizing the evolution of the molecular axis alignment. The latter being theoretically predicted based on molecular constants, rotational temperature and pump pulse characteristics, the dynamical parameters C_{KQ}^{LM} were extracted from the measured $\beta_2(t)$ and $\beta_4(t)$ parameters, leading *via* a nonlinear regression to the dipole moments magnitude and phases for $l = 0$ –3 partial waves, in total 6 moduli and 5 phases (relative values) (see Formalism). The missing phase connecting σ and π channels, which would require circularly polarized light, was computed. The retrieved complex valued dipole moments were found in fair agreement with those obtained from previous calculations³⁹³ and from rotationally resolved studies,³⁸³ the sensitivity of the (t, E) time-energy maps enabling to discriminate between the two previous sets of data. Crucial is the very accurate, low noise primary data for the TRPADs.

Impulsive laser alignment, avoiding resonant conditions, was pushed to its limit to allow the full determination of complex dipole matrix elements, and to reconstruct MFPADs for ionization of N_2 in the X, A and B channels, by recording LFPADs from a broad rotational wavepacket.³¹ High harmonics of a 267 nm driving field, H_5 at 23.3 eV and H_7 at 32.6 eV, were employed to record PADs for the three channels by sampling the delay relative to the alignment pulse in 150 time steps of 67 fs covering 10 ps. The large amount of data was used initially to reconstruct the time dependent moments describing the axis alignment $P(\theta, t)$ from the $\beta_L(t)$ measured parameters of the PADs, $S(\theta, t) = \sum_{LM} \beta_{LM}(t) Y_{LM}(\theta, 0)$, $L = 0, 2, 4, 6$. From

$$P(\theta, t) = \sum_{KQ} A_{K,Q}(t) Y_{KQ}(\theta, 0) \quad \beta_{LM}(t) = \sum_{KQ} C_{KQ}^{LM} A_{K,Q}(t)$$

($M, Q = 0$ in the present experiment) both the aligning pulse optimal parameters, which determine the $A_{KQ}(t)$ moments, and the coupling terms C_{KQ}^{LM} can be determined. The latter can be expressed as a quadratic expression in the dipole transition moments, which can be finally retrieved with iterative nonlinear fitting. While in principle a well-defined mathematical procedure, very accurate PADs need to be recorded, and elaborate optimization cycles of fitting to determine the dipole matrix elements are needed. Best results were obtained for the X channel, which produced six complex dipoles, while more noisy data, and weaker dependence of the PADs on $P(\theta, t)$ for the A and B channels produced some ambiguities. The obtained dipoles allow for the calculation of the full MFPADs, also for orientations different from that in the experiment, and comparison with *ab initio* computed ones showed very good agreement for the X channel, more mixed results for the A one. While this experiment involves a linear $D_{\infty h}$ molecule, and low energy electrons, so the number of effective dipoles is very limited, the method is fully general, allowing a “complete experiment” to be performed. The reconstruction of

MFPADs from TRPADs in polyatomic has been further theoretically analyzed.³⁹⁴ The key observation is that both LFPADs and MFPADs depend linearly from the dipole products $d_{\text{Elm}\gamma}^{(-)} d_{\text{El'm'}\gamma'}^{(-)*}$ (see formalism), and once the C_{KQ}^{LM} have been extracted in LF one can retrieve the corresponding coefficients in MF, and express the full MFPAD through them, bypassing the determination of the individual dipole matrix elements, by solving systems of linear equations (with generalized inverses in case of singularities) instead of quadratic regressions. This was demonstrated for N_2 and C_2H_4 , making explicit use of molecular symmetry.³⁹⁴

Momentum analysis of LFPAD anisotropies relying on ultra-fast time-energy-angle resolved observables, when an electron wave-packet launched by a pump pulse is probed by valence ionization, was recently proposed as a new method to access molecular frame electronic coherences, as demonstrated for dissociation of excited states of the NH_3 molecule.^{1,395}

Inner-shell ionization of aligned molecules: Femtosecond photoelectron diffraction

The availability of ultra-intense X-ray femtosecond pulses at XFEL facilities motivated the implementation of experiments extending the previously described “photoelectron diffraction from within” scheme, aiming at following time-dependent structural changes in molecules with femtosecond time and Angström spatial resolution,³² as an alternative to X-ray photon diffraction or ultra-fast photoelectron diffraction based on electron guns. At XFELs, the method benefits from the extended photon energy range accessible to induce inner-shell localized photoionization processes up to few hundreds of eV above ionization thresholds, and relies on their comparatively large cross sections of the order of 10^{-20} cm^2 . The optimal strategy to take advantage of the huge intensity available (10^{13} ph per pulse) resulting in hundreds of electrons per pulse, and account for the low repetition rate of the order of 100 Hz in the FEL context *e.g.* at LCLS,³⁹⁶ was to work with an assembly of aligned and/or oriented molecules and use a dedicated double sided VMI spectrometer such as the CAMP endstation (see Exp. section).¹⁵⁸ The latter was designed to measure simultaneously both high-energy electrons and ion fragments, thereby taking the electron diffraction data extracted from the PADs while continuously monitoring the degree of alignment of the molecules, as well as identifying the fragmentation channels. First experiments were performed at LCLS on rotationally cold adiabatically aligned and mixed-field oriented polyatomic molecules such as 1-ethynyl-4-fluorobenzene ($\text{C}_8\text{H}_5\text{F}$) or 1,4-dibromobenzene ($\text{C}_6\text{H}_4\text{Br}_2$),^{397,398} and the PADs for core-shell ionization of the halogen atom interpreted based on comparison with DFT calculations, taking into account a degree of alignment up to $\langle \cos^2 \theta_{2D} \rangle = 0.89$. They demonstrated the feasibility of photoelectron diffraction at XFELs for femtosecond time-resolved molecular structure imaging provided that some issues are achieved, such as *e.g.* an excellent degree of molecular alignment (larger than 0.95) preferably in field-free conditions to avoid the influence of the alignment laser on the studied processes, or the control of contamination of the target by molecular clusters.¹⁸¹

A similar project aiming at X-ray photoelectron diffraction (XPD) was pursued at the SPring-8 Angström Compact free-electron



Laser (SACLA).³⁹⁹ In an experiment analyzing XPD PADs recorded for adiabatically aligned I₂ molecules ionized by the SACLA XFEL 140 eV above threshold of the I 2p_{3/2} inner-shell (IP = 4.557 keV) an I–I internuclear distance elongated by about 10% of its equilibrium value of 2.66 Å was revealed⁴⁰⁰ and interpreted as bond length softening due to multi-photon excitation of the I₂ molecule in presence of the moderately intense alignment Nd:YAG laser. The need for field free conditions and for a degree of alignment significantly larger than those reported ($\langle \cos^2 \theta_{2D} \rangle = 0.734$) was as well underlined in order to achieve precise XPD studies.

The situation has evolved recently with the advent of high repetition rates in the MHz range at the European XFEL,¹⁴³ and becoming soon available at LCLS-II,¹⁴⁴ opening access to coincidence experiments and related diagnostics as illustrated above.

Strong field ionization in the molecular frame

Within the development of attosecond science, strong field ionization of molecules is a topic of widespread interest. The complex photoelectron angular distribution resulting from the interaction of an intense IR femtosecond laser field with a molecule can be assigned to contributions of the ionization process as described by the well-known three step model:^{401,402} within a period of the driving femtosecond optical field, a valence electron wavepacket is extracted from the target through tunnel ionization or above threshold ionization, accelerated in vacuum by the laser field, and partly driven back to the parent ion, where it encounters rescattering or radiative recombination.

Strong field ionization. Since tunnel ionization dealing with outermost electronic orbitals is generally non-dissociative, the ability to align molecules is crucial to access MFPAD snapshots or more generally molecular frame photoelectron momentum distributions (MFPMDs), required as well when the axial recoil approximation is questionable in dissociative ionization of polyatomic molecules. In the last fifteen years several questions have been addressed, triggered by the structured PMDs induced by strong field linearly polarized light filtering direct ionization *via* selection of low photoelectron momenta,⁴⁰³ or by means of circularly polarized light which suppresses recollision of the freed electron with the parent ion. Imprint of outermost molecular orbitals in 3D PMDs was demonstrated for SFI of field-free aligned or anti-aligned linear molecules (N₂, O₂) using a COLTRIMS set-up and a TiSa laser (10¹⁴ W cm⁻² 40 fs 30 kHz),⁴⁰⁴ revealed in particular when considering the normalized differences of the two momentum distributions $I_{\text{diff}} = (I_{\text{align}} - I_{\text{antialign}})/(I_{\text{align}} + I_{\text{antialign}})$. Nodal planes of outermost electronic orbitals of 3D adiabatically aligned and oriented benzonitrile molecules were identified in PMDs,^{405,406} and permanent dipole moments and polarizabilities were extracted for OCS polar molecules,^{405,407} supported by tunneling ionization theory.⁴⁰⁸ 3D MFPMDs for SFI of naphthalene were obtained by tomographic reconstruction using a variable alignment elliptically polarized YAG laser.⁴⁰⁹

The dependence of strong field ionization yields on the angle between the principal molecular axis, or the most

polarizable axis, and the ionizing field is a more restricted observable, however pursued in different contexts to improve the description of molecular tunneling ionization based on a detailed comparison with theoretical models.^{410–414} It was as well considered to unveil multiple electronic SFI channels for above-threshold ionization (ATI) of *e.g.* 1,3-butadiene molecules.⁴¹⁵

Beyond the molecular frame dependence of the nascent photoelectron momentum distribution probing tunnel ionization, the imprints of the emitted photoelectron wavepacket onto laser-driven electron recollision,⁴¹⁶ photoelectron holography⁴¹⁷ or laser-induced electron diffraction^{418–420} are further scrutinized in recent studies involving small molecules, as well as more complex polyatomic molecules such as 1–3 butadiene (C₄H₆)⁴¹⁶ or the prototypical biomolecule indole (C₈H₇N), a major ultraviolet-absorbing chromophore of proteins.⁴²¹

Laser induced electron diffraction. Considering the overall PADs or PMDs arising from strong field ionization of randomly oriented then aligned molecules, a number of recent studies focus on the specific contribution of the broadband electron wave packet formed by the returning electrons elastically scattered, and in particular back-scattered by the parent ion, setting the conditions of Laser Induced Electron Diffraction (LIED).^{422–425} Depending on the wavelength of the mid-IR ionizing laser field, electron energy extends up to a few hundreds of eV (10 Up where Up is the ponderomotive energy). Based on theoretical modelling, the influence of the driving strong laser field on the electron momentum distributions can be deconvoluted, providing field free elastic differential cross sections (DCS) for the electron recolliding with the molecular ion, characteristic of electron diffraction patterns.⁴²⁶ This was experimentally demonstrated in the reported 3D PMDs for N₂ and O₂ which highlighted angle dependent oscillations of the I_{diff} normalized PMD differences outlined above,⁴⁰⁴ for different p_r recollision electron momenta, revealing molecular interatomic distances.

A first quantitative LIED application to molecular dynamics for a sample of randomly aligned N₂ and O₂ molecules was demonstrated by varying the wavelength of the 1 kHz mid-IR ionizing laser (1.7–2–2.3 μm), which is equivalent to taking snapshots of the molecular structure at different recollision times (variation of few fs) within an intrapulse pump–probe scheme, probing a bond length contraction of 0.1 Å with a sensitivity of 5 picometre (pm) for the O₂ case due to the vibrational motion subsequent to tunnel ionization.⁴²⁷ After extraction of the field-free DCS from the measured PMDs based on the quantitative rescattering theory (QRS),^{424,428,429} bond lengths (R) were retrieved from the comparison of measured molecular contrast factors $\sim (\sin qR)/qR$, reflecting the molecular interference term of the rescattered electron momentum distribution, as a function of the momentum transfer $q = 2p_r \sin(\theta_r/2)$, with computed ones based on the independent-atom model (IAM).⁴²⁹ Geometrical structure and bond lengths were also obtained for unaligned polyatomic molecules such as benzene⁴³⁰ and ethylene⁴³¹ using a similar approach. It is worth noting that for randomly oriented neutral small molecules the ionization step generally induces partial alignment, though the contrast of the diffraction features after rescattering is improved



for prepared laser aligned molecules, thereby relating each step of the process resulting in the studied PAD or PMD to the molecular frame.

Combining a 160 kHz mid-IR (3.1 μm) source with a reaction microscope,¹³⁶ LIED was exploited *e.g.* to retrieve multiple bond lengths in impulsively aligned acetylene,⁴³² image bond breaking in di-ionized acetylene,⁴³³ or non-adiabatic Renner–Teller effects in the neutral $\text{CS}_2(\text{B}^1\text{B}_2)$ excited state of carbonyl disulfide,⁴³⁴ relying on the electron–ion coincidence to decipher between different reaction pathways. Unlike the case of CS_2 where vibronic excitation induced by the driving field prior to ionization was inferred,⁴³⁴ as illustrated in Fig. 7, LIED of randomly oriented molecules carbonyl sulfide OCS using mid-IR (2 μm) around a comparable 10^{14} W cm^{-2} intensity and a high energy VMI imaging electrons up to 500 eV, the geometry and bond distances of the OCS molecule extracted with a precision better than ± 5 pm were found in good agreement with the known structure of ground-state OCS.⁴³⁵ Additionally, the classical rescattering model can also be invoked to associate a specific returning time to the measured electron rescattering energy, reaching a sub-femtosecond temporal resolution for the geometrical structure.^{432,434}

Through these examples LIED demonstrates its ability for probing photoinduced molecular dynamics in the MF with femto-to-attosecond temporal and sub-Å spatial resolutions.

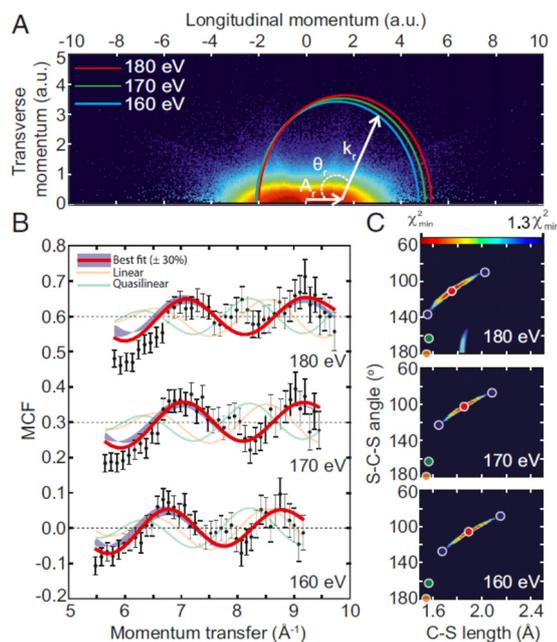


Fig. 7 LIED imaging of laser-induced vibronic excitation in CS_2 .⁴³⁴ (A) measured photoelectron momentum distribution providing field free DCSs for different electron returning energies E_R using the QRS theory, (B) molecular contrast factors for $E_R = 160, 170, 180$ eV: (dots) experimental, and (red line) computed for the geometric structure leading to the MCF closest to the experiment, (C) (red dots) retrieved most probable symmetrically stretched and bent geometry of CS_2^+ . Figure reproduced from Fig. 1 of ref. 434 with permission from Proc. Natl. Acad. Sci. USA under Creative Commons Attribution 4.0 International license (<http://creativecommons.org/licenses/by/4.0/>).

A careful account of the influence of the three ionization, propagation and rescattering steps, in particular the MF orientation relative to the polarization⁴³⁶ or the multielectron character⁴¹⁹ governing the properties of the released electron wavepacket is to be considered for the interpretation of the recorded 3D PMDs. For more complex molecules, structure information retrieval requires extending the tractability of the QRS theory and IAM model algorithms based on the θ_r dependence of PMDs at fixed k_r . The measured PMDs can alternatively be analyzed through a Fourier transform variant of LIED based on energy spectra of back-scattered electrons ($\theta_r = 180^\circ$): FT-LIED,^{418,437,438} *i.e.* fixed-angle broadband laser driven electron scattering (FABLES),⁴³⁹ or through implementation of more general retrieval methods,⁴⁴⁰ as recently demonstrated combining LIED with machine learning to image molecules such as Fenchone.⁴⁴¹

If pump–probe femtosecond experiments where LIED acts as a probe of ultrafast dynamics launched by a coherent pump pulse has not been yet fully demonstrated, recent time-resolved results in the picosecond range have been reported based on the analysis of PMDs acquired with a VMI spectrometer.^{442,443} LIED and photoelectron holography were investigated simultaneously through the PMDs for SFI of nitrogen monoxide NO, recorded at different delays after launching a rotational wave packet in NO, tracking the coupling between valence-shell electronic and rotational dynamics.⁴⁴² The measured and computed field-free DCSs extracted from laser induced electron recollision PADs for SFI of Iodine I_2 weakly bound excited state in the regime of low-energy electron scattering were shown to display comparable features evolving with the time-delay relative to the prompt excitation of a vibrational wave packet, assigned to the role of a shape resonance and its energy dependence to the molecular internuclear distance.⁴⁴³

Perspective

As illustrated through the range of experiments addressed in this perspective, the scope of angle resolved molecular photoelectron spectroscopy has broadly expanded in the last two decades, uncovering light–matter interactions in different field strength regimes and involving targets of increasing complexity as illustrated *e.g.* by the characterization of chiral objects. Access to these new regimes challenges as well theoretical descriptions. The richness of the PAD observables, and in particular MFPADs, emerges from the quantum interference imprint carried by the photoelectron scattering states and unveiled in angular distributions. They provide highly valuable information on the electronic structure of stationary molecular states and photoionization dynamics influenced by electronic correlation, resonances or fundamental symmetries, accessing the final continuum partial wave phases and transition amplitudes of the relevant operator (electric dipole in the simplest case), ideally up to so-called complete experiment where all matrix elements up to a given final angular momentum are reconstructed. MFPADs, PA-MFPADs, or PMDs are also currently interpreted as diffraction



patterns of the scattered electron wave revealing molecular geometrical structures, in particular when emission occurs from a localized atomic orbital subsequent to X-ray ionization, or results from strong field tunnel ionization in LIED. This methodological corpus builds up a strong potential for future studies of molecular structure and dynamics in real time.^{1,444}

From the experimental side, new challenges are driven by the impressive achievements of light sources, both at large-scale XFEL facilities and based on advanced table-top laser sources, pushing to higher intensity and higher energy photons, ever shorter pulse duration, with increasing repetition rates in the range of several hundreds of kHz up to MHz, but also ever more complex pulses and nonclassical light, characterized by fields structured in the four-dimensional space-time, with strong inhomogeneity of all light parameters.^{234,236} Angular distributions from ionization with specially tailored fields are mostly untouched. Beside HHG attosecond XUV pulses, X-ray laser-enhanced attosecond pulses are in progress at LCLS and European XFEL, as characterized using photoelectron angular streaking spectroscopy.⁴⁴⁵ Concurrently, the continuous progress in large solid angle acceptance, efficient position and time sensitive detectors will benefit multicoincidence experiments, in general allowing the study of low cross section minority channels. It includes *e.g.* extensions to electron–ion–photon coincidences, favoured by enhanced photon detection efficiency combined with the time and position capabilities,^{161,446} foreseen in particular in the hard X-ray domain where radiative decay contributes to the relaxation of core–hole excited states.²⁹⁵ Moreover the sharpening alignment and orientation techniques for gas phase molecules combined with VMI based detection will render MFPADS much more routinely available for complex systems.

This instrumental context will extend significantly the range and the achievements of temporally resolved studies aiming at characterizing in real time molecular structure and intramolecular dynamics triggered by photoabsorption and probed by photoionization,¹ *i.e.* featuring a so-called “molecular movie”. Such processes involve the relaxation dynamics of excited molecular states to lower potential energy surfaces *via* nonadiabatic couplings, and to vibrational motion giving rise to bond stretching/opening, isomerization, and dissociation, generally underlying chemical bond making and breaking, or even electronic wavepacket motion or charge migration.^{447–449} Despite the popularity of challenging pump–probe experiments, quite few probe the dynamics beyond the simple photoelectron spectra, often leading to a limited characterization of the internal dynamics, with remaining ambiguities. The rich information embodied in angularly resolved studies from oriented molecules will be greatly beneficial to fully characterize the electronic states involved, their coupling with nuclear motion,⁴⁵⁰ and the electron wavepacket coherences^{395,451,452} and bifurcations, up to now quite elusive, both in valence excitation and ionization with broad pulses.

Recent results obtained at the European XFEL for single-pulse two-photon sequential core ionization pave the way for MF angle-resolved X-ray pump X-ray probe experiments temporally resolved at the femtosecond time scale, with perspectives to observe *e.g.* coherent electron–hole dynamics on the

attosecond scale. In strong field ionization, implementing LIED, which also features an intrapulse pump–probe scheme, as an effective pump–probe tool to characterize molecular structure in real time is in progress.

Probing the photoionization dynamics in the MF in real time with attosecond accuracy, involving the overlap of an XUV attosecond pulse and a phase-locked NIR femtosecond pulse *e.g.* in the RABBITT interference scheme, fostered by recent developments, should be further investigated. The achievement of coherent XUV pulses, *e.g.* at the fundamental ω and second harmonic 2ω as demonstrated at the FERMI seeded FEL,⁴⁵³ enables recording interferences between one-photon and two-photon quantum paths,⁴⁵⁴ revealing LF angle resolved phase differences of the corresponding photoionization amplitudes, opening new perspectives for molecules.²⁹⁰

Meanwhile, the complementarity between ultrafast time domain studies and high resolution energy domain achieved at synchrotrons remains quite relevant and attractive, as illustrated *e.g.* by the recent developments of MF angle resolved photoionization time delays.

Another direction is the push to multiphoton effects in the high energy domains with XFELS. Double (multiple) core holes and decays will be studied, including time delays for sequential process, exploiting photoelectron and Auger in coincidence. The hard X-ray region, where a number of unexplored issues are anticipated,⁴⁵⁵ has been barely explored in molecules. A number of new effects, like non dipole, nuclear recoil and Compton scattering,⁴⁵⁶ although individually understood in basic terms, contribute together and will open a new window in molecular interactions. Compton scattering from individual orbitals in oriented molecules can provide a new and direct way of orbital imaging.^{457,458} Nonlinear process like stimulated Compton scattering will become available.³⁷⁵ Other double ionization studies will be extended into the high kinetic energy domain, where the two electron continuum simplifies and new windows may be opened to the imaging of the electronic wavefunction.

One obvious fostered perspective is the extension of LF or MF angle resolved PES studies to more complex molecules (finite systems), supported by both recent advances in Coulomb explosion imaging,⁴⁵⁹ and the fast improvement of alignment/orientation protocols.¹⁹³ This direction also implies specialized methods to produce gas phase targets from different species as mentioned earlier, such as fragile molecules, radicals, positive and negative ions, clusters, nanoparticles, high temperature vapors, and further selection of conformers.¹⁰⁴ Further developments exploring the boundary between gas phase and condensed systems are *e.g.* aqueous solutions in droplets or liquid jets, surfactant layer structure at liquid–vapor interface, and molecules adsorbed on surfaces.

Besides characterization of the electronic structure of the target, like orbital composition and imaging, a deeper insight into many-body effects, both in the bound and continuum states, will be pursued, through precise experiments on multi-electron effects in ionization, in particular multiply excited initial and final states with different excitation mechanisms. Their understanding is a fundamental problem of current



References

- 1 M. S. Schuurman and V. Blanchet, *Phys. Chem. Chem. Phys.*, 2022, DOI: [10.1039/D1CP05885A](https://doi.org/10.1039/D1CP05885A).
- 2 D. Dill, *J. Chem. Phys.*, 1976, **65**, 1130–1133.
- 3 N. Chandra, *J. Phys. B: At. Mol. Phys.*, 1987, **20**, 3405–3415.
- 4 A. V. Golovin, N. A. Cherepkov and V. V. Kuznetsov, *Z. Phys. D - Atoms Molec. Clusters*, 1992, **24**, 371–375.
- 5 H. Park and R. N. Zare, *J. Chem. Phys.*, 1996, **104**, 4554–4567.
- 6 S. K. Semenov and N. A. Cherepkov, *J. Phys. B: At. Mol. Opt. Phys.*, 2009, **42**, 085101.
- 7 V. V. Kuznetsov, S. K. Semenov and N. A. Cherepkov, *J. Chem. Phys.*, 2011, **134**, 134301.
- 8 R. R. Lucchese and D. Dowek, *Attosecond and XUV Physics: Ultrafast Dynamics and Spectroscopy*, ed. T. Schultz and M. Vrakking, Wiley Online Library, 2014, pp. 293–320.
- 9 E. P. Wigner, *Phys. Rev.*, 1955, **98**, 145–147.
- 10 J. M. Dahlström, A. L'Huillier and A. Maquet, *J. Phys. B: At. Mol. Opt. Phys.*, 2012, **45**, 183001.
- 11 J. M. Dahlström, D. Guénot, K. Klünder, M. Gisselbrecht, J. Mauritsson, A. L'Huillier, A. Maquet and R. Taïeb, *Chem. Phys.*, 2013, **414**, 53–64.
- 12 R. Pazourek, S. Nagele and J. Burgdörfer, *Rev. Mod. Phys.*, 2015, **87**, 765–802.
- 13 P. Hockett, E. Frumker, D. M. Villeneuve and P. B. Corkum, *J. Phys. B: At. Mol. Opt. Phys.*, 2016, **49**, 095602.
- 14 D. Baykusheva and H. J. Wörner, *J. Chem. Phys.*, 2017, **146**, 124306.
- 15 R. R. Lucchese, A. Lafosse, J. C. Brenot, P. M. Guyon, J. C. Houver, M. Lebech, G. Raseev and D. Dowek, *Phys. Rev. A*, 2002, **65**, 020702.
- 16 A. Lafosse, J. C. Brenot, P. M. Guyon, J. C. Houver, A. V. Golovin, M. Lebech, D. Dowek, P. Lin and R. R. Lucchese, *J. Chem. Phys.*, 2002, **117**, 8368–8384.
- 17 M. Lebech, J. C. Houver, A. Lafosse, D. Dowek, C. Alcaraz, L. Nahon and R. R. Lucchese, *J. Chem. Phys.*, 2003, **118**, 9653–9663.
- 18 X.-J. Liu, R. R. Lucchese, A. N. Grum-Grzhimailo, Y. Morishita, N. Saito, G. Prümper and K. Ueda, *J. Phys. B: At. Mol. Opt. Phys.*, 2007, **40**, 485–496.
- 19 R. R. Lucchese, R. Montuoro, A. N. Grum-Grzhimailo, X.-J. Liu, G. Prümper, Y. Morishita, N. Saito and K. Ueda, *J. Electron Spectrosc. Relat. Phenom.*, 2007, **155**, 95–99.
- 20 D. Dowek and R. R. Lucchese, *Dynamical Processes in Atomic and Molecular Physics*, Bentham Bussum The Netherlands, 2012, vol. 39, pp. 57–95.
- 21 K. L. Reid, D. J. Leahy and R. N. Zare, *Phys. Rev. Lett.*, 1992, **68**, 3527–3530.
- 22 N. A. Cherepkov, G. Raseev, J. Adachi, Y. Hikosaka, K. Ito, S. Motoki, M. Sano, K. Soejima and A. Yagishita, *J. Phys. B: At. Mol. Opt. Phys.*, 2000, **33**, 4213–4236.
- 23 O. Geßner, Y. Hikosaka, B. Zimmermann, A. Hempelmann, R. R. Lucchese, J. H. D. Eland, P.-M. Guyon and U. Becker, *Phys. Rev. Lett.*, 2002, **88**, 193002.
- 24 P. Hockett, M. Wollenhaupt, C. Lux and T. Baumert, *Phys. Rev. Lett.*, 2014, **112**, 223001.
- 25 C. S. Trevisan, C. W. McCurdy and T. N. Rescigno, *J. Phys. B: At. Mol. Opt. Phys.*, 2012, **45**, 194002.
- 26 D. Toffoli, R. R. Lucchese, M. Lebech, J. C. Houver and D. Dowek, *J. Chem. Phys.*, 2007, **126**, 054307.
- 27 J. G. Underwood and K. L. Reid, *J. Chem. Phys.*, 2000, **113**, 1067–1074.
- 28 K. L. Reid, *Annu. Rev. Phys. Chem.*, 2003, **54**, 397–424.
- 29 K. L. Reid, *Mol. Phys.*, 2012, **110**, 131–147.
- 30 H. Stapelfeldt and T. Seideman, *Rev. Mod. Phys.*, 2003, **75**, 543–557.
- 31 C. Marceau, V. Makhija, D. Platzer, A. Y. Naumov, P. B. Corkum, A. Stolow, D. M. Villeneuve and P. Hockett, *Phys. Rev. Lett.*, 2017, **119**, 083401.
- 32 F. Krasniqi, B. Najjari, L. Strüder, D. Rolles, A. Voitkiv and J. Ullrich, *Phys. Rev. A*, 2010, **81**, 033411.
- 33 M. Kazama, T. Fujikawa, N. Kishimoto, T. Mizuno, J. Adachi and A. Yagishita, *Phys. Rev. A*, 2013, **87**, 063417.
- 34 C. Yu and X. Wang, *Phys. Rev. A*, 2019, **100**, 063422.
- 35 J. W. Cooper, *Phys. Rev. A*, 1990, **42**, 6942–6945.
- 36 A. N. Grum-Grzhimailo, *J. Phys. B: At. Mol. Opt. Phys.*, 2003, **36**, 2385–2407.
- 37 R. Kosloff, *J. Phys. Chem.*, 1988, **92**, 2087–2100.
- 38 A. Castro, M. A. L. Marques and A. Rubio, *J. Chem. Phys.*, 2004, **121**, 9.
- 39 A. C. Brown, G. S. J. Armstrong, J. Benda, D. D. A. Clarke, J. Wragg, K. R. Hamilton, Z. Mašín, J. D. Gorfinkiel and H. W. van der Hart, *Comput. Phys. Commun.*, 2020, **250**, 107062.
- 40 N. Tancogne-Dejean, M. J. T. Oliveira, X. Andrade, H. Appel, C. H. Borca, G. Le Breton, F. Buchholz, A. Castro, S. Corni, A. A. Correa, U. De Giovannini, A. Delgado, F. G. Eich, J. Flick, G. Gil, A. Gomez, N. Helbig, H. Hübener, R. Jestädt, J. Jornet-Somoza, A. H. Larsen, I. V. Lebedeva, M. Lüders, M. A. L. Marques, S. T. Ohlmann, S. Pipolo, M. Rampp, C. A. Rozzi, D. A. Strubbe, S. A. Sato, C. Schäfer, I. Theophilou, A. Welden and A. Rubio, *J. Chem. Phys.*, 2020, **152**, 124119.
- 41 L. B. Madsen, L. A. A. Nikolopoulos and P. Lambropoulos, *Eur. Phys. J. D*, 2000, **10**, 67–79.
- 42 A. Palacios, C. W. McCurdy and T. N. Rescigno, *Phys. Rev. A*, 2007, **76**, 043420.
- 43 G. Grell, O. Kühn and S. I. Bokarev, *Phys. Rev. A*, 2019, **100**, 042512.
- 44 N. Chandra and M. Chakraborty, *J. Chem. Phys.*, 1992, **97**, 236–244.
- 45 N. Chandra and M. Chakraborty, *J. Chem. Phys.*, 1993, **99**, 7314–7330.
- 46 S. K. Semenov, V. V. Kuznetsov, N. A. Cherepkov, P. Bolognesi, V. Feyer, A. Lahmam-Bennani, M. E. S. Casagrande and L. Avaldi, *Phys. Rev. A*, 2007, **75**, 032707.
- 47 A. Szabo and N. S. Ostlund, *Modern quantum chemistry: introduction to advanced electronic structure theory*, Courier Corporation, 2012.
- 48 T. Helgaker, P. Jorgensen and J. Olsen, *Molecular electronic-structure theory*, John Wiley & Sons, 2014.



- 49 B. O. Roos, R. Lindh, P. Malmqvist, V. Veryazov and P. O. Widmark, *Multiconfigurational Quantum Chemistry*, Wiley-Blackwell, 2016.
- 50 F. Aquilante, J. Autschbach, A. Baiardi, S. Battaglia, V. A. Borin, L. F. Chibotaru, I. Conti, L. De Vico, M. Delcey, I. F. Galván, N. Ferré, L. Freitag, M. Garavelli, X. Gong, S. Knecht, E. D. Larsson, R. Lindh, M. Lundberg, P. Å. Malmqvist, A. Nenov, J. Norell, M. Odellius, M. Olivucci, T. B. Pedersen, L. Pedraza-González, Q. M. Phung, K. Pierloot, M. Reiher, I. Schapiro, J. Segarra-Martí, F. Segatta, L. Seijo, S. Sen, D.-C. Sergentu, C. J. Stein, L. Ungur, M. Vacher, A. Valentini and V. Veryazov, *J. Chem. Phys.*, 2020, **152**, 214117.
- 51 B. N. C. Tenorio, A. Ponzi, S. Coriani and P. Decleva, *Molecules*, 2022, **27**, 1203.
- 52 L. S. Cederbaum and W. Domcke, in *Advances in Chemical Physics*, ed. I. Prigogine and S. A. Rice, John Wiley & Sons, Inc., Hoboken, NJ, USA, 1977, pp. 205–344.
- 53 J. V. Ortiz, *J. Chem. Phys.*, 2020, **153**, 070902.
- 54 J. Schirmer and A. B. Trofimov, *J. Chem. Phys.*, 2004, **120**, 11449–11464.
- 55 S. Banerjee and A. Y. Sokolov, *J. Chem. Phys.*, 2019, **151**, 224112.
- 56 A. L. Dempwolff, M. Hodecker and A. Dreuw, *J. Chem. Phys.*, 2022, **156**, 054114.
- 57 J. F. Stanton and R. J. Bartlett, *J. Chem. Phys.*, 1993, **98**, 7029–7039.
- 58 C. Melania Oana and A. I. Krylov, *J. Chem. Phys.*, 2007, **127**, 234106.
- 59 T. Moitra, A. C. Paul, P. Decleva, H. Koch and S. Coriani, *Phys. Chem. Chem. Phys.*, 2022, **24**, 8329–8343.
- 60 M. Ehara, J. Hasegawa and H. Nakatsuji, in *Theory and Applications of Computational Chemistry*, ed. C. E. Dykstra, G. Frenking, K. S. Kim and G. E. Scuseria, Elsevier, Amsterdam, 2005, pp. 1099–1141.
- 61 R. Parr and W. Yang, *Density Functional Theory of Atoms and Molecules*, New York, Oxford Univ. Press, 1989.
- 62 K. Burke and L. O. Wagner, *Int. J. Quantum Chem.*, 2013, **113**, 96–101.
- 63 K. Burke, J. Werschnik and E. K. U. Gross, *J. Chem. Phys.*, 2005, **123**, 062206.
- 64 M. Stener, G. Fronzoni and P. Decleva, *J. Chem. Phys.*, 2005, **122**, 234301.
- 65 S. I. Bokarev and O. Kühn, *Wiley Interdiscip. Rev.: Comput. Mol. Sci.*, 2020, **10**, e1433.
- 66 C. Daniel, L. González and F. Neese, *Phys. Chem. Chem. Phys.*, 2021, **23**, 2533–2534.
- 67 L. S. Cederbaum, W. Domcke, J. Schirmer and W. V. Niessen, in *Advances in Chemical Physics*, ed. I. Prigogine and S. A. Rice, John Wiley & Sons, Inc., Hoboken, NJ, USA, 1986, pp. 115–159.
- 68 A. D. O. Bawagan and E. R. Davidson, *Advances in Chemical Physics*, John Wiley & Sons, Ltd, 1999, pp. 215–266.
- 69 R. E. Stratmann and R. R. Lucchese, *J. Chem. Phys.*, 1995, **102**, 8493–8505.
- 70 P. V. Demekhin, A. Ehresmann and V. L. Sukhorukov, *J. Chem. Phys.*, 2011, **134**, 024113.
- 71 V. P. Majety, A. Zielinski and A. Scrinzi, *New J. Phys.*, 2015, **17**, 063002.
- 72 C. Marante, M. Klinker, I. Corral, J. González-Vázquez, L. Argenti and F. Martín, *J. Chem. Theory Comput.*, 2017, **13**, 499–514.
- 73 Z. Mašín, J. Benda, J. D. Gorfinkiel, A. G. Harvey and J. Tennyson, *Comput. Phys. Commun.*, 2020, **249**, 107092.
- 74 P. Decleva, M. Stener and D. Toffoli, *Molecules*, 2022, **27**, 2026.
- 75 A. Ponzi, C. Angeli, R. Cimiraglia, S. Coriani and P. Decleva, *J. Chem. Phys.*, 2014, **140**, 204304.
- 76 K. H. Johnson, in *Advances in Quantum Chemistry*, ed. P.-O. Löwdin, Academic Press, 1973, vol. 7, pp. 143–185.
- 77 D. Dill and J. L. Dehmer, *J. Chem. Phys.*, 1974, **61**, 692–699.
- 78 K. Hatada, K. Hayakawa, M. Benfatto and C. R. Natoli, *J. Phys.: Condens. Matter*, 2010, **22**, 185501.
- 79 R. R. Lucchese, K. Takatsuka and V. McKoy, *Phys. Rep.*, 1986, **131**, 147–221.
- 80 T. N. Rescigno, C. W. McCurdy, A. E. Orel and B. H. Lengsfeld, in *Computational Methods for Electron-Molecule Collisions*, ed. W. M. Huo and F. A. Gianturco, Plenum Press, New York, 1995, pp. 1–44.
- 81 P. G. Burke, *R-matrix theory of atomic collisions: Application to atomic, molecular and optical processes*, Springer Science & Business Media, 2011, vol. 61.
- 82 P. Descouvemont and D. Baye, *Rep. Prog. Phys.*, 2010, **73**, 036301.
- 83 C. Froese Fischer and M. Idrees, *Comput. Phys.*, 1989, **3**, 53.
- 84 M. Brosolo and P. Decleva, *Chem. Phys.*, 1992, **159**, 185–196.
- 85 M. Kazama, T. Fujikawa, N. Kishimoto, T. Mizuno, J. Adachi and A. Yagishita, *Phys. Rev. A*, 2013, **87**, 063417.
- 86 D. Toffoli and P. Decleva, *J. Chem. Theory Comput.*, 2016, **12**, 4996–5008.
- 87 N. M. Novikovskiy, A. N. Artemyev, D. V. Rezvan, B. M. Lagutin and P. V. Demekhin, *J. Phys. B: At., Mol. Opt. Phys.*, 2022, **55**, 175001.
- 88 T. Sato and K. L. Ishikawa, *Phys. Rev. A*, 2013, **88**, 023402.
- 89 A. F. Al-Refai and J. Tennyson, *Comput. Phys. Commun.*, 2017, **221**, 53–62.
- 90 F. A. Gianturco, R. R. Lucchese and N. Sanna, *J. Chem. Phys.*, 1994, **100**, 6464–6471.
- 91 A. P. Natalense and R. R. Lucchese, *J. Chem. Phys.*, 1999, **111**, 5344–5348.
- 92 I. Powis, *J. Chem. Phys.*, 2000, **112**, 301–310.
- 93 I. Powis, *J. Phys. Chem. A*, 2000, **104**, 878–882.
- 94 Y. Suzuki and T. Suzuki, *J. Phys. Chem. A*, 2008, **112**, 402–411.
- 95 H. Ganjitarbar, G. A. Garcia, L. Nahon and I. Powis, *J. Chem. Phys.*, 2020, **153**, 034302.
- 96 T. Piteša, M. Sapunar, A. Ponzi, M. F. Gelin, N. Došlić, W. Domcke and P. Decleva, *J. Chem. Theory Comput.*, 2021, **17**, 5098–5109.
- 97 F. Ota, S. Abe, K. Hatada, K. Ueda, S. Díaz-Tendero and F. Martín, *Phys. Chem. Chem. Phys.*, 2021, **23**, 20174–20182.
- 98 M. Williams, R. Forbes, H. Weir, K. Veyrinas, R. J. MacDonell, A. E. Boguslavskiy, M. S. Schuurman,



- A. Stolow and T. J. Martinez, *J. Phys. Chem. Lett.*, 2021, **12**, 6363–6369.
- 99 R. Forbes, S. P. Neville, M. A. B. Larsen, A. Röder, A. E. Boguslavskiy, R. Lausten, M. S. Schuurman and A. Stolow, *J. Phys. Chem. Lett.*, 2021, **12**, 8541–8547.
- 100 U. Even, *EPJ tech. instrum.*, 2015, **2**, 17.
- 101 F. Filsinger, G. Meijer, H. Stapelfeldt, H. N. Chapman and J. Küpper, *Phys. Chem. Chem. Phys.*, 2011, **13**, 2076–2087.
- 102 M. H. M. Janssen and I. Powis, *Phys. Chem. Chem. Phys.*, 2014, **16**, 856–871.
- 103 L. Nahon, G. A. Garcia and I. Powis, *J. Electron Spectrosc. Relat. Phenom.*, 2015, **204**, 322–334.
- 104 Y.-P. Chang, D. A. Horke, S. Trippel and J. Küpper, *Int. Rev. Phys. Chem.*, 2015, **34**, 557–590.
- 105 M. Shaikh, X. Liu, K. Amini, T. Steinle and J. Biegert, *Rev. Sci. Instrum.*, 2021, **92**, 104103.
- 106 J. Eland, *Int. J. Mass Spectrom. Ion Phys.*, 1972, **8**, 143–151.
- 107 C. J. Danby and J. H. D. Eland, *Int. J. Mass Spectrom. Ion Phys.*, 1972, **8**, 153–161.
- 108 J. Eland, *J. Chem. Phys.*, 1979, **70**, 2926–2933.
- 109 E. Shigemasa, J. Adachi, M. Oura and A. Yagishita, *Phys. Rev. Lett.*, 1995, **74**, 359–362.
- 110 J. Eland and E. Duerr, *Chem. Phys.*, 1998, **229**, 1–11.
- 111 P. Downie and I. Powis, *Phys. Rev. Lett.*, 1999, **82**, 2864.
- 112 M. Takahashi, J. P. Cave and J. H. D. Eland, *Rev. Sci. Instrum.*, 2000, **71**, 1337–1344.
- 113 A. Lafosse, M. Lebeck, J. C. Brenot, P. M. Guyon, O. Jagutzki, L. Spielberger, M. Vervloet, J. C. Houver and D. Doweck, *Phys. Rev. Lett.*, 2000, **84**, 5987–5990.
- 114 J. A. Davies, R. E. Continetti, D. W. Chandler and C. C. Hayden, *Phys. Rev. Lett.*, 2000, **84**, 5983–5986.
- 115 C. Bomme, R. Guillemin, T. Marin, L. Journal, T. Marchenko, D. Doweck, N. Trcera, B. Pilette, A. Avila, H. Ringuenet, R. K. Kushawaha and M. Simon, *Rev. Sci. Instrum.*, 2013, **84**, 103104.
- 116 R. Dörner, V. Mergel, O. Jagutzki, L. Spielberger, J. Ullrich, R. Moshhammer and H. Schmidt-Böcking, *Phys. Rep.*, 2000, **330**, 95–192.
- 117 J. Ullrich, R. Moshhammer, A. Dorn, R. Dörner, L. P. H. Schmidt and H. Schmidt-Böcking, *Rep. Prog. Phys.*, 2003, **66**, 1463–1545.
- 118 T. Jahnke, Th Weber, T. Osipov, A. L. Landers, O. Jagutzki, L. P. H. Schmidt, C. L. Cocke, M. H. Prior, H. Schmidt-Böcking and R. Dörner, *J. Electron Spectrosc. Relat. Phenom.*, 2004, **141**, 229–238.
- 119 M. Gisselbrecht, A. Huetz, M. Lavollée, T. Reddish and D. Secombe, *Rev. Sci. Instrum.*, 2005, **76**, 013105.
- 120 R. N. Zare, *Mol. Photochem.*, 1972, **4**, 1–37.
- 121 J. A. Beswick and R. N. Zare, *J. Chem. Phys.*, 2008, **129**, 164315.
- 122 O. Jagutzki, V. Mergel, K. Ullmann-Pfleger, L. Spielberger, U. Spillmann, R. Dörner and H. Schmidt-Böcking, *Nucl. Instrum. Methods Phys. Res., Sect. A*, 2002, **477**, 244–249.
- 123 O. Jagutzki, A. Cerezo, A. Czasch, R. Dörner, M. Hattas, M. Huang, V. Mergel, U. Spillmann, K. Ullmann-Pfleger and T. Weber, *IEEE Trans. Nucl. Sci.*, 2002, **49**, 2477–2483.
- 124 RoentDek Handels GmbH, <http://www.roentdek.com>.
- 125 S. Matoba, R. Takahashi, C. Io, T. Koizumi and H. Shiromaru, *Jpn. J. Appl. Phys.*, 2011, **50**, 112201.
- 126 K. Fehre, D. Trojanowskaja, J. Gatzke, M. Kunitski, F. Trinter, S. Zeller, L. P. H. Schmidt, J. Stohner, R. Berger and A. Czasch, *Rev. Sci. Instrum.*, 2018, **89**, 045112.
- 127 T. Weber, M. Weckenbrock, M. Balsler, L. Schmidt, O. Jagutzki, W. Arnold, O. Hohn, M. Schöffler, E. Arenholz, T. Young, T. Osipov, L. Foucar, A. D. Fanis, R. Díez Muiño, H. Schmidt-Böcking, C. L. Cocke, M. H. Prior and R. Dörner, *Phys. Rev. Lett.*, 2003, **90**, 153003.
- 128 M. Lebeck, J. C. Houver and D. Doweck, *Rev. Sci. Instrum.*, 2002, **73**, 1866–1874.
- 129 A. Vredenburg, W. G. Roeterdink and M. H. M. Janssen, *Rev. Sci. Instrum.*, 2008, **79**, 063108.
- 130 U. Ablikim, C. Bomme, T. Osipov, H. Xiong, R. Obaid, R. C. Bilodeau, N. G. Kling, I. Dumitriu, S. Augustin, S. Pathak, K. Schnorr, D. Kilcoyne, N. Berrah and D. Rolles, *Rev. Sci. Instrum.*, 2019, **90**, 055103.
- 131 O. Gessner, A. Lee, J. P. Shaffer, H. Reisler, S. V. Levchenko, A. I. Krylov, J. G. Underwood, H. Shi, A. L. East and D. Wardlaw, *Science*, 2006, **311**, 219–222.
- 132 A. Vredenburg, W. G. Roeterdink and M. H. M. Janssen, *J. Chem. Phys.*, 2008, **128**, 204311.
- 133 S. Marggi Poullain, C. Elkharrat, W. B. Li, K. Veyrinas, J. C. Houver, C. Cornaggia, T. N. Rescigno, R. R. Lucchese and D. Doweck, *J. Phys. B: At. Mol. Phys.*, 2014, **47**, 124024.
- 134 M. Sabbar, S. Heuser, R. Boge, M. Lucchini, L. Gallmann, C. Cirelli and U. Keller, *Rev. Sci. Instrum.*, 2014, **85**, 103113.
- 135 J. Biegert, F. Calegari, N. Dudovich, F. Quéré and M. Vrakking, *J. Phys. B: At. Mol. Phys.*, 2021, **54**, 070201.
- 136 B. Wolter, M. G. Pullen, M. Baudisch, M. Sclafani, M. Hemmer, A. Senftleben, C. D. Schröter, J. Ullrich, R. Moshhammer and J. Biegert, *Phys. Rev. X*, 2015, **5**, 021034.
- 137 D. Hammerland, P. Zhang, S. Kühn, P. Jojart, I. Seres, V. Zuba, Z. Varallyay, D. Charalambidis, K. Osvay and T. T. Luu, *J. Phys. B: At. Mol. Phys.*, 2019, **52**, 23LT01.
- 138 M. Osolodkov, F. J. Furch, F. Schell, P. Šušnjar, F. Cavalcante, C. S. Menoni, C. P. Schulz, T. Witting and M. J. Vrakking, *J. Phys. B: At. Mol. Phys.*, 2020, **53**, 194003.
- 139 T. Witting, M. Osolodkov, F. Schell, F. Morales, S. Patchkovskii, P. Šušnjar, F. H. M. Cavalcante, C. S. Menoni, C. P. Schulz, F. J. Furch and M. J. Vrakking, *Optica*, 2022, **9**, 145–151.
- 140 S. Mikaelsson, J. Vogelsang, C. Guo, I. Sytcevic, A.-L. Viotti, F. Langer, Y.-C. Cheng, S. Nandi, W. Jin, A. Olofsson, R. Weissenbilder, J. Mauritsson, A. L'Huillier, M. Gisselbrecht and C. L. Arnold, *Nanophotonics*, 2021, **10**, 117–128.
- 141 L. Young, K. Ueda, M. Gühr, P. H. Bucksbaum, M. Simon, S. Mukamel, N. Rohringer, K. C. Prince, C. Masciovecchio, M. Meyer, A. Rudenko, D. Rolles, C. Bostedt, M. Fuchs, D. A. Reis, R. Santra, H. Kapteyn, M. Murnane, H. Ibrahim, F. Légaré, M. Vrakking, M. Isinger, D. Kroon, M. Gisselbrecht, A. L'Huillier, H. J. Wörner and S. R. Leone, *J. Phys. B: At. Mol. Phys.*, 2018, **51**, 032003.



- 142 K. Ueda, E. Sokell, S. Schippers, F. Aumayr, H. Sadeghpour, J. Burgdörfer, C. Lemell, X.-M. Tong, T. Pfeifer, F. Calegari, A. Palacios, F. Martin, P. Corkum, G. Sansone, E. V. Gryzlova, A. N. Grum-Grzhimailo, M. N. Piancastelli, P. M. Weber, T. Steinle, K. Amini, J. Biegert, N. Berrah, E. Kukk, R. Santra, A. Müller, D. Dowek, R. R. Lucchese, C. W. McCurdy, P. Bolognesi, L. Avaldi, T. Jahnke, M. S. Schöffler, R. Dörner, Y. Mairesse, L. Nahon, O. Smirnova, T. Schlathölter, E. E. B. Campbell, J.-M. Rost, M. Meyer and K. A. Tanaka, *J. Phys. B: At. Mol. Phys.*, 2019, **52**, 171001.
- 143 W. Decking, S. Abeghyan, P. Abramian, A. Abramsky, A. Aguirre, C. Albrecht, P. Alou, M. Altarelli, P. Altmann, K. Amyan, V. Anashin, E. Apostolov, K. Appel, D. Auguste, V. Ayvazyan, S. Baark, F. Babies, N. Baboi, P. Bak, V. Balandin, R. Baldinger, B. Baranasic, S. Barbanotti, O. Belikov, V. Belokurov, L. Belova, V. Belyakov, S. Berry, M. Bertucci, B. Beutner, A. Block, M. Blöcher, T. Böckmann, C. Bohm, M. Böhnert, V. Bondar, E. Bondarchuk, M. Bonezzi, P. Borowiec, C. Bösch, U. Bösenberg, A. Bosotti, R. Böspflug, M. Bousonville, E. Boyd, Y. Bozhko, A. Brand, J. Branlard, S. Briechle, F. Brinker, S. Brinker, R. Brinkmann, S. Brockhauser, O. Brovko, H. Brück, A. Brüdgam, L. Butkowski, T. Büttner, J. Calero, E. Castro-Carballo, G. Cattalanotto, J. Charrier, J. Chen, A. Cherepenko, V. Cheskidov, M. Chiodini, A. Chong, S. Choroba, M. Chorowski, D. Churanov, W. Cichalewski, M. Clausen, W. Clement, C. Cloué, J. A. Cobos, N. Coppola, S. Cunis, K. Czuba, M. Czwalińska, B. D'Almagne, J. Dammann, H. Danared, A. de Zubiaurre Wagner, A. Delfs, T. Delfs, F. Dietrich, T. Dietrich, M. Dohlus, M. Dommach, A. Donat, X. Dong, N. Doynikov, M. Dressel, M. Duda, P. Duda, H. Eckoldt, W. Ehsan, J. Eidam, F. Eints, C. Engling, U. Englisch, A. Ermakov, K. Escherich, J. Eschke, E. Saldin, M. Faesing, A. Fallou, M. Felber, M. Fenner, B. Fernandes, J. M. Fernández, S. Feuker, K. Filippakopoulos, K. Floettmann, V. Fogel, M. Fontaine, A. Francés, I. F. Martin, W. Freund, T. Freyermuth, M. Friedland, L. Fröhlich, M. Fusetti, J. Fydrych, A. Gallas, O. García, L. Garcia-Tabares, G. Geloni, N. Gerasimova, C. Gerth, P. Geßler, V. Gharibyan, M. Gloor, J. Glowinkowski, A. Goessel, Z. Gołębiewski, N. Golubeva, W. Grabowski, W. Graeff, A. Grebentsov, M. Grecki, T. Grevsmuehl, M. Gross, U. Grosse-Wortmann, J. Grünert, S. Grunewald, P. Grzegory, G. Feng, H. Guler, G. Gusev, J. L. Gutierrez, L. Hagge, M. Hamberg, R. Hanneken, E. Harms, I. Hartl, A. Hauberg, S. Hauf, J. Hauschildt, J. Hauser, J. Havlicek, A. Hedqvist, N. Heidbrook, F. Hellberg, D. Henning, O. Hensler, T. Hermann, A. Hidvégi, M. Hierholzer, H. Hintz, F. Hoffmann, M. Hoffmann, M. Hoffmann, Y. Holler, M. Hüning, A. Ignatenko, M. Ilchen, A. Iluk, J. Iversen, J. Iversen, M. Izquierdo, L. Jachmann, N. Jardon, U. Jastrow, K. Jensch, J. Jensen, M. Ježabek, M. Jidda, H. Jin, N. Johansson, R. Jonas, W. Kaabi, D. Kaefer, R. Kammering, H. Kapitza, S. Karabekyan, S. Karstensen, K. Kasprzak, V. Katalev, D. Keese, B. Keil, M. Kholopov, M. Killenberger, B. Kitaev, Y. Klimchenko, R. Klos, L. Knebel, A. Koch, M. Koepke, S. Köhler, W. Köhler, N. Kohlstrunk, Z. Konopkova, A. Konstantinov, W. Kook, W. Koprek, M. Körfer, O. Korth, A. Kosarev, K. Kosiński, D. Kostin, Y. Kot, A. Kotarba, T. Kozak, V. Kozak, R. Kramert, M. Krasilnikov, A. Krasnov, B. Krause, L. Kravchuk, O. Krebs, R. Kretschmer, J. Kreutzkamp, O. Kröplin, K. Krzysik, G. Kube, H. Kuehn, N. Kujala, V. Kulikov, V. Kuzminych, D. La Civita, M. Lacroix, T. Lamb, A. Lancetov, M. Larsson, D. Le Pinvidic, S. Lederer, T. Lensch, D. Lenz, A. Leuschner, F. Levenhagen, Y. Li, J. Liebing, L. Lilje, T. Limberg, D. Lipka, B. List, J. Liu, S. Liu, B. Lorbeer, J. Lorkiewicz, H. H. Lu, F. Ludwig, K. Machau, W. Maciocha, C. Madec, C. Magueur, C. Maiano, I. Maksimova, K. Malcher, T. Maltezopoulos, E. Mamoshkina, B. Manschwetus, F. Marcellini, G. Marinkovic, T. Martinez, H. Martirosyan, W. Maschmann, M. Maslov, A. Matheisen, U. Mavric, J. Meißner, K. Meissner, M. Messerschmidt, N. Meyners, G. Michalski, P. Michelato, N. Mildner, M. Moe, F. Moglia, C. Mohr, S. Mohr, W. Möller, M. Mommerz, L. Monaco, C. Montiel, M. Moretti, I. Morozov, P. Morozov, D. Mross, J. Mueller, C. Müller, J. Müller, K. Müller, J. Munilla, A. Münnich, V. Muratov, O. Napoly, B. Näser, N. Nefedov, R. Neumann, R. Neumann, N. Ngada, D. Noelle, F. Obier, I. Okunev, J. A. Oliver, M. Omet, A. Oppelt, A. Ottmar, M. Oublaïd, C. Pagani, R. Paparella, V. Paramonov, C. Peitzmann, J. Penning, A. Perus, F. Peters, B. Petersen, A. Petrov, I. Petrov, S. Pfeiffer, J. Pflüger, S. Philipp, Y. Pienaud, P. Pierini, S. Pivovarov, M. Planas, E. Pławski, M. Pohl, J. Polinski, V. Popov, S. Prat, J. Prenting, G. Priebe, H. Pryschelski, K. Przygoda, E. Pyata, B. Racky, A. Rathjen, W. Ratuschni, S. Regnaud-Campderros, K. Rehlich, D. Reschke, C. Robson, J. Roeber, M. Roggli, J. Rothenburg, E. Rusiński, R. Rybaniec, H. Sahling, M. Salmani, L. Samoylova, D. Sanzone, F. Saretzki, O. Sawlanski, J. Schaffran, H. Schlarb, M. Schlösser, V. Schlott, C. Schmidt, F. Schmidt-Foehre, M. Schmitz, M. Schmökel, T. Schnautz, E. Schneidmiller, M. Scholz, B. Schöneburg, J. Schultze, C. Schulz, A. Schwarz, J. Sekutowicz, D. Sellmann, E. Semenov, S. Serkez, D. Sertore, N. Shehzad, P. Shemarykin, L. Shi, M. Sienkiewicz, D. Sikora, M. Sikorski, A. Silenzi, C. Simon, W. Singer, X. Singer, H. Sinn, K. Sinram, N. Skvorodnev, P. Smirnow, T. Sommer, A. Sorokin, M. Stadler, M. Steckel, B. Steffen, N. Steinhau-Kühl, F. Stephan, M. Stodulski, M. Stolper, A. Sulimov, R. Susen, J. Świerblewski, C. Sydlo, E. Syresin, V. Sytchev, J. Szuba, N. Tesch, J. Thie, A. Thiebault, K. Tiedtke, D. Tischhauser, J. Tolkiehn, S. Tomin, F. Tonisch, F. Toral, I. Torbin, A. Trapp, D. Treyer, G. Trowitzsch, T. Trublet, T. Tschentscher, F. Ullrich, M. Vannoni, P. Varela, G. Varghese, G. Vashchenko, M. Vasic, C. Vazquez-Velez, A. Verguet, S. Vilcins-Czvitkovits, R. Villanueva, B. Visentin, M. Viti, E. Vogel, E. Volobuev, R. Wagner, N. Walker,



- T. Wamsat, H. Weddig, G. Weichert, H. Weise, R. Wennendorf, M. Werner, R. Wichmann, C. Wiebers, M. Wiencek, T. Wilksen, I. Will, L. Winkelmann, M. Winkowski, K. Wittenburg, A. Witzig, P. Wlk, T. Wohlenberg, M. Wojciechowski, F. Wolff-Fabris, G. Wrochna, K. Wrona, M. Yakopov, B. Yang, F. Yang, M. Yurkov, I. Zagorodnov, P. Zalden, A. Zavadtsev, D. Zavadtsev, A. Zhirnov, A. Zhukov, V. Ziemann, A. Zolotov, N. Zolotukhina, F. Zummack and D. Zybin, *Nat. Photonics*, 2020, **14**, 391–397.
- 144 J. N. Galayda, *The LCLS-II: A high power upgrade to the LCLS*, SLAC National Accelerator Lab., Menlo Park, CA (United States), 2018.
- 145 D. W. Chandler, P. L. Houston and D. H. Parker, *J. Chem. Phys.*, 2017, **147**, 013601.
- 146 A. T. J. B. Eppink and D. H. Parker, *Rev. Sci. Instrum.*, 1997, **68**, 3477–3484.
- 147 V. Dribinski, A. Ossadtchi, V. A. Mandelshtam and H. Reisler, *Rev. Sci. Instrum.*, 2002, **73**, 2634–2642.
- 148 G. A. Garcia, L. Nahon and I. Powis, *Rev. Sci. Instrum.*, 2004, **75**, 4989–4996.
- 149 T. Horio and T. Suzuki, *Rev. Sci. Instrum.*, 2009, **80**, 013706.
- 150 C. Vallance, M. Brouard, A. Lauer, C. S. Slater, E. Halford, B. Winter, S. J. King, J. W. L. Lee, D. E. Pooley, I. Sedgwick, R. Turchetta, A. Nomerotski, J. J. John and L. Hill, *Phys. Chem. Chem. Phys.*, 2014, **16**, 383–395.
- 151 S. K. Lee, Y. F. Lin, S. Lingenfelter, L. Fan, A. H. Winney and W. Li, *J. Chem. Phys.*, 2014, **141**, 221101.
- 152 M. Wollenhaupt, M. Krug, J. Köhler, T. Bayer, C. Sarpe-Tudoran and T. Baumert, *Appl. Phys. B*, 2009, **95**, 245–259.
- 153 J. Maurer, D. Dimitrovski, L. Christensen, L. B. Madsen and H. Stapelfeldt, *Phys. Rev. Lett.*, 2012, **109**, 123001.
- 154 P. Johnsson, W. Siu, A. Gijsbertsen, J. Verhoeven, A. S. Meijer, W. van der Zande and M. J. J. Vrakking, *J. Mod. Opt.*, 2008, **55**, 2693–2709.
- 155 P. O’Keeffe, V. Feyer, P. Bolognesi, M. Coreno, C. Callegari, G. Cautero, A. Moise, K. C. Prince, R. Richter, R. Sergo, M. Alagia, M. de Simone, A. Kivimäki, M. Devetta, T. Mazza, P. Piseri, V. Lyamayev, R. Katzy, F. Stienkemeier, Y. Ovcharenko, T. Möller and L. Avaldi, *Nucl. Instrum. Methods Phys. Res., Sect. B*, 2012, **284**, 69–73.
- 156 G. A. Garcia, L. Nahon, C. J. Harding, E. A. Mikajlo and I. Powis, *Rev. Sci. Instrum.*, 2005, **76**, 053302.
- 157 N. G. Kling, D. Paul, A. Gura, G. Laurent, S. De, H. Li, Z. Wang, B. Ahn, C. H. Kim, T. K. Kim, I. V. Litvinyuk, C. L. Cocke, I. Ben-Itzhak, D. Kim and M. F. Kling, *J. Inst.*, 2014, **9**, P05005.
- 158 L. Strüder, S. Epp, D. Rolles, R. Hartmann, P. Holl, G. Lutz, H. Soltau, R. Eckart, C. Reich, K. Heinzinger, C. Thamm, A. Rudenko, F. Krasniqi, K.-U. Kühnel, C. Bauer, C.-D. Schröter, R. Moshhammer, S. Techert, D. Miessner, M. Porro, O. Hälker, N. Meidinger, N. Kimmel, R. Andritschke, F. Schopper, G. Weidenspointner, A. Ziegler, D. Pietschner, S. Herrmann, U. Pietsch, A. Walenta, W. Leitenberger, C. Bostedt, T. Möller, D. Rupp, M. Adolph, H. Graafsma, H. Hirsemann, K. Gärtner, R. Richter, L. Foucar, R. L. Shoeman, I. Schlichting and J. Ullrich, *Nucl. Instrum. Methods Phys. Res., Sect. A*, 2010, **614**, 483–496.
- 159 K. Nakajima, T. Teramoto, H. Akagi, T. Fujikawa, T. Majima, S. Minemoto, K. Ogawa, H. Sakai, T. Togashi, K. Tono, S. Tsuru, K. Wada, M. Yabashi and A. Yagishita, *Sci. Rep.*, 2015, **5**, 14065.
- 160 Z. Vager, R. Naaman and E. Kanter, *Science*, 1989, **244**, 426–431.
- 161 A. Tremsin and J. Vallergera, *Radiat. Meas.*, 2020, **130**, 106228.
- 162 G. Basnayake, Y. Ranathunga, S. K. Lee and W. Li, *J. Phys. B: At., Mol. Opt. Phys.*, 2022, **55**, 023001.
- 163 J. Long, F. J. Furch, J. Durá, A. S. Tremsin, J. Vallergera, C. P. Schulz, A. Rouzée and M. J. Vrakking, *J. Chem. Phys.*, 2017, **147**, 013919.
- 164 A. Zhao, M. van Beuzekom, B. Bouwens, D. Byelov, I. Chakaberia, C. Cheng, E. Maddox, A. Nomerotski, P. Svirha, J. Visser, V. Vrba and T. Weinacht, *Rev. Sci. Instrum.*, 2017, **88**, 113104.
- 165 C. Schouder, A. S. Chatterley, M. Johnny, F. Hübschmann, A. F. Al-Refaie, F. Calvo, J. Küpper and H. Stapelfeldt, *J. Phys. B: At. Mol. Phys.*, 2021, **54**, 184001.
- 166 G. A. Garcia, H. Soldi-Lose and L. Nahon, *Rev. Sci. Instrum.*, 2009, **80**, 023102.
- 167 A. Bodi, M. Johnson, T. Gerber, Z. Gengeliczki, B. Sztáray and T. Baer, *Rev. Sci. Instrum.*, 2009, **80**, 034101.
- 168 A. Bodi, P. Hemberger, T. Gerber and B. Sztáray, *Rev. Sci. Instrum.*, 2012, **83**, 083105.
- 169 G. A. Garcia, B. K. Cunha de Miranda, M. Tia, S. Daly and L. Nahon, *Rev. Sci. Instrum.*, 2013, **84**, 053112.
- 170 C. S. Lehmann, N. B. Ram and M. H. M. Janssen, *Rev. Sci. Instrum.*, 2012, **83**, 093103.
- 171 L. Fan, S. K. Lee, Y.-J. Tu, B. Mignolet, D. Couch, K. Dorney, Q. Nguyen, L. Wooldridge, M. Murnane, F. Remacle, H. B. Schlegel and W. Li, *J. Chem. Phys.*, 2017, **147**, 013920.
- 172 L. J. Frasinski, *J. Phys. B: At., Mol. Opt. Phys.*, 2016, **49**, 152004.
- 173 C. P. Koch, M. Lemesko and D. Sugny, *Rev. Mod. Phys.*, 2019, **91**, 035005.
- 174 K. Lin, I. Tutunnikov, J. Ma, J. Qiang, L. Zhou, O. Faucher, Y. Prior, I. S. Averbukh and J. Wu, *Adv. Photonics*, 2020, **2**, 024002.
- 175 K. L. Reid, *Philos. Trans. R. Soc., A*, 2018, **376**, 20170158.
- 176 J. J. Larsen, K. Hald, N. Bjerre, H. Stapelfeldt and T. Seideman, *Phys. Rev. Lett.*, 2000, **85**, 2470–2473.
- 177 F. Rosca-Pruna and M. Vrakking, *Phys. Rev. Lett.*, 2001, **87**, 153902.
- 178 J. L. Hansen, J. H. Nielsen, C. B. Madsen, A. T. Lindhardt, M. P. Johansson, T. Skrydstруп, L. B. Madsen and H. Stapelfeldt, *J. Chem. Phys.*, 2012, **136**, 204310.
- 179 K. Amini, R. Boll, A. Lauer, M. Burt, J. W. L. Lee, L. Christensen, F. Brauße, T. Mullins, E. Saveljev, U. Ablikim, N. Berrah, C. Bomme, S. Düsterer, B. Erk, H. Höppner, P. Johnsson, T. Kierspel, F. Krecinic, J. Küpper, M. Müller, E. Müller, H. Redlin, A. Rouzée, N. Schirmel, J. Thøgersen, S. Techert, S. Toleikis, R. Treusch, S. Trippel, A. Ulmer, J. Wiese, C. Vallance,



- 217 J. A. DeVine, M. L. Weichman, B. Laws, J. Chang, M. C. Babin, G. Balerdi, C. Xie, C. L. Malbon, W. C. Lineberger, D. R. Yarkony, R. W. Field, S. T. Gibson, J. Ma, H. Guo and D. M. Neumark, *Science*, 2017, **358**, 336–339.
- 218 K. A. Larsen, R. Y. Bello, R. R. Lucchese, T. N. Rescigno, C. W. McCurdy, D. S. Slaughter and T. Weber, *Phys. Rev. A*, 2020, **102**, 063118.
- 219 M. Eckstein, C.-H. Yang, F. Frassetto, L. Poletto, G. Sansone, M. J. J. Vrakking and O. Kornilov, *Phys. Rev. Lett.*, 2016, **116**, 163003.
- 220 M. Fushitani, S. T. Pratt, D. You, S. Saito, Y. Luo, K. Ueda, H. Fujise, A. Hishikawa, H. Ibrahim, F. Légaré, P. Johnsson, J. Peschel, E. R. Simpson, A. Olofsson, J. Mauritsson, P. A. Carpeggiani, P. K. Maroju, M. Moiola, D. Ertel, R. Shah, G. Sansone, T. Csizmadia, M. Dumergue, N. G. Harshitha, S. Kühn, C. Callegari, O. Plekan, M. Di Fraia, M. B. Danailov, A. Demidovich, L. Giannessi, L. Raimondi, M. Zangrando, G. De Ninno, P. R. Ribič and K. C. Prince, *J. Chem. Phys.*, 2021, **154**, 144305.
- 221 V. Loriot, A. Marciniak, S. Nandi, G. Karras, M. Hervé, E. Constant, E. Plésiat, A. Palacios, F. Martín and F. Lépine, *J. Phys. Photonics*, 2020, **2**, 024003.
- 222 C. Z. Bisgaard, O. J. Clarkin, G. Wu, A. M. D. Lee, O. Gefšner, C. C. Hayden and A. Stolow, *Science*, 2009, **323**, 1464.
- 223 P. Hockett, C. Z. Bisgaard, O. J. Clarkin and A. Stolow, *Nat. Phys.*, 2011, **7**, 612–615.
- 224 Y.-I. Suzuki and T. Suzuki, *J. Chem. Phys.*, 2012, **137**, 194314.
- 225 T. Horio, R. Spesyvtsev, K. Nagashima, R. A. Ingle, Y. Suzuki and T. Suzuki, *J. Chem. Phys.*, 2016, **145**, 044306.
- 226 J. O. F. Thompson, L. Saalbach, S. W. Crane, M. J. Paterson and D. Townsend, *J. Chem. Phys.*, 2015, **142**, 114309.
- 227 T. Suzuki, private communication.
- 228 L. Poisson, P. Roubin, S. Coussan, B. Soep and J.-M. Mestdagh, *J. Am. Chem. Soc.*, 2008, **130**, 2974–2983.
- 229 R. J. Squibb, M. Sapunar, A. Ponzi, R. Richter, A. Kivimäki, O. Plekan, P. Finetti, N. Sisourat, V. Zhaunerchyk, T. Marchenko, L. Journal, R. Guillemin, R. Cucini, M. Coreno, C. Grazioli, M. Di Fraia, C. Callegari, K. C. Prince, P. Decleva, M. Simon, J. H. D. Eland, N. Došlić, R. Feifel and M. N. Piancastelli, *Nat. Commun.*, 2018, **9**, 63.
- 230 N. Kotsina, M. Candelaresi, L. Saalbach, M. M. Zawadzki, S. W. Crane, C. Sparling and D. Townsend, *Phys. Chem. Chem. Phys.*, 2020, **22**, 4647–4658.
- 231 R. E. Goetz, T. A. Isaev, B. Nikoobakht, R. Berger and C. P. Koch, *J. Chem. Phys.*, 2017, **146**, 024306.
- 232 C. Rosales-Guzmán, B. Ndagano and A. Forbes, *J. Opt.*, 2018, **20**, 123001.
- 233 H. Kang, A. S. Maxwell, D. Trabert, X. Lai, S. Eckart, M. Kunitski, M. Schöffler, T. Jahnke, X. Bian, R. Dörner and C. F. M. de Faria, *Phys. Rev. A*, 2020, **102**, 013109.
- 234 O. V. Angelsky, A. Y. Bekshaev, S. G. Hanson, C. Y. Zenkova, I. I. Mokhun and Z. Jun, *Front. Phys.*, 2020, **8**, 114.
- 235 C. Figueira de Morisson Faria and A. S. Maxwell, *Rep. Prog. Phys.*, 2020, **83**, 034401.
- 236 A. Forbes, M. de Oliveira and M. R. Dennis, *Nat. Photonics*, 2021, **15**, 253–262.
- 237 S. Hartweg, B. L. Yoder, G. A. Garcia, L. Nahon and R. Signorell, *Phys. Rev. Lett.*, 2017, **118**, 103402.
- 238 D. K. Božanić, G. A. Garcia, O. Sublemontier, J. Pajović, V. Djoković and L. Nahon, *J. Phys. Chem. C*, 2020, **124**, 24500–24512.
- 239 T. Suzuki, *J. Chem. Phys.*, 2019, **151**, 090901.
- 240 R. Signorell and B. Winter, *Phys. Chem. Chem. Phys.*, 2022, **24**, 13438–13460.
- 241 R. Dupuy, J. Filser, C. Richter, R. Seidel, F. Trinter, T. Buttersack, C. Nicolas, J. Bozek, U. Hergenhahn and H. Oberhofer, *Phys. Chem. Chem. Phys.*, 2022, **24**, 4796–4808.
- 242 B. Ritchie, *Phys. Rev. A*, 1976, **13**, 1411–1415.
- 243 N. Böwering, T. Lischke, B. Schmidtke, N. Müller, T. Khalil and U. Heinzmann, *Phys. Rev. Lett.*, 2001, **86**, 1187–1190.
- 244 S. Beaulieu, A. Ferré, R. Géneaux, R. Canonge, D. Descamps, B. Fabre, N. Fedorov, F. Légaré, S. Petit and T. Ruchon, *New J. Phys.*, 2016, **18**, 102002.
- 245 A. D. Müller, E. Kutscher, A. N. Artemyev and P. V. Demekhin, *J. Chem. Phys.*, 2020, **152**, 044302.
- 246 M. N. Pohl, S. Malerz, F. Trinter, C. Lee, C. Kolbeck, I. Wilkinson, S. Thürmer, D. M. Neumark, L. Nahon, I. Powis, G. Meijer, B. Winter and U. Hergenhahn, *Phys. Chem. Chem. Phys.*, 2022, **24**, 8081–8092.
- 247 T. Müller, K. B. Wiberg and P. H. Vaccaro, *J. Phys. Chem. A*, 2000, **104**, 5959–5968.
- 248 C. Meinert, A. D. Garcia, J. Topin, N. C. Jones, M. Diekmann, R. Berger, L. Nahon, S. V. Hoffmann and U. J. Meierhenrich, *Nat. Commun.*, 2022, **13**, 502.
- 249 S. Daly, F. Rosu and V. Gabelica, *Science*, 2020, **368**, 1465–1468.
- 250 F. Saito and P. R. Schreiner, *Eur. J. Org. Chem.*, 2020, 6328–6339.
- 251 P. Decleva, *Chemistry*, 2022, **4**, 31–41.
- 252 D. Di Tommaso, M. Stener, G. Fronzoni and P. Decleva, *ChemPhysChem*, 2006, **7**, 924–934.
- 253 J. Dupont, V. Lepère, A. Zehnacker, S. Hartweg, G. A. Garcia and L. Nahon, *J. Phys. Chem. Lett.*, 2022, **13**, 2313–2320.
- 254 R. Hadidi, D. K. Božanić, H. Ganjtabar, G. A. Garcia, I. Powis and L. Nahon, *Commun. Chem.*, 2021, **4**, 72.
- 255 R. Hadidi, D. K. Bozanic, G. A. Garcia and L. Nahon, *Adv. Phys.: X*, 2018, **3**, 1477530.
- 256 B. Darquié, N. Saleh, S. K. Tokunaga, M. Srebro-Hooper, A. Ponzi, J. Autschbach, P. Decleva, G. A. Garcia, J. Crassous and L. Nahon, *Phys. Chem. Chem. Phys.*, 2021, **23**, 24140–24153.
- 257 D. Catone, M. Stener, P. Decleva, G. Contini, N. Zema, T. Prospero, V. Feyer, K. C. Prince and S. Turchini, *Phys. Rev. Lett.*, 2012, **108**, 083001.
- 258 D. Catone, S. Turchini, M. Stener, P. Decleva, G. Contini, T. Prospero, V. Feyer, K. C. Prince and N. Zema, *Rend. Fis. Acc. Lincei*, 2013, **24**, 269–275.
- 259 G. A. Garcia, L. Nahon, S. Daly and I. Powis, *Nat. Commun.*, 2013, **4**, 2132.
- 260 G. A. Garcia, H. Dossmann, L. Nahon, S. Daly and I. Powis, *ChemPhysChem*, 2017, **18**, 500–512.



- 336 X.-J. Liu, H. Fukuzawa, T. Teranishi, A. De Fanis, M. Takahashi, H. Yoshida, A. Cassimi, A. Czasch, L. Schmidt, R. Dörner, K. Wang, B. Zimmermann, V. McKoy, I. Koyano, N. Saito and K. Ueda, *Phys. Rev. Lett.*, 2008, **101**, 083001.
- 337 R. R. Lucchese, H. Fukuzawa, X.-J. Liu, T. Teranishi, N. Saito and K. Ueda, *J. Phys. B: At., Mol. Opt. Phys.*, 2012, **45**, 194014.
- 338 T. Osipov, T. N. Rescigno, T. Weber, S. Miyabe, T. Jahnke, A. S. Alnaser, M. P. Hertlein, O. Jagutzki, L. P. H. Schmidt, M. Schöffler, L. Foucar, S. Schössler, T. Havermeier, M. Odenweller, S. Voss, B. Feinberg, A. L. Landers, M. H. Prior, R. Dörner, C. L. Cocke and A. Belkacem, *J. Phys. B: At., Mol. Opt. Phys.*, 2008, **41**, 091001.
- 339 M. S. Schöffler, J. Titze, N. Petridis, T. Jahnke, K. Cole, L. P. H. Schmidt, A. Czasch, D. Akoury, O. Jagutzki, J. B. Williams, N. A. Cherepkov, S. K. Semenov, C. W. McCurdy, T. N. Rescigno, C. L. Cocke, T. Osipov, S. Lee, M. H. Prior, A. Belkacem, A. L. Landers, H. Schmidt-Böcking, T. Weber and R. Dörner, *Science*, 2008, **320**, 920–923.
- 340 S. K. Semenov, M. S. Schöffler, J. Titze, N. Petridis, T. Jahnke, K. Cole, L. P. H. Schmidt, A. Czasch, D. Akoury, O. Jagutzki, J. B. Williams, T. Osipov, S. Lee, M. H. Prior, A. Belkacem, A. L. Landers, H. Schmidt-Böcking, T. Weber, N. A. Cherepkov and R. Dörner, *Phys. Rev. A*, 2010, **81**, 043426.
- 341 H. Sann, T. Havermeier, C. Müller, H.-K. Kim, F. Trinter, M. Waitz, J. Voigtsberger, F. Sturm, T. Bauer, R. Wallauer, D. Schneider, M. Weller, C. Goihl, J. Tross, K. Cole, J. Wu, M. S. Schöffler, H. Schmidt-Böcking, T. Jahnke, M. Simon and R. Dörner, *Phys. Rev. Lett.*, 2016, **117**, 243002.
- 342 J. P. Cryan, J. M. Glowina, J. Andreasson, A. Belkacem, N. Berrah, C. I. Blaga, C. Bostedt, J. Bozek, C. Buth, L. F. DiMauro, L. Fang, O. Gessner, M. Guehr, J. Hajdu, M. P. Hertlein, M. Hoener, O. Kornilov, J. P. Marangos, A. M. March, B. K. McFarland, H. Merdji, V. S. Petrović, C. Raman, D. Ray, D. Reis, F. Tarantelli, M. Trigo, J. L. White, W. White, L. Young, P. H. Bucksbaum and R. N. Coffee, *Phys. Rev. Lett.*, 2010, **105**, 083004.
- 343 G. Kastirke, M. S. Schöffler, M. Weller, J. Rist, R. Boll, N. Anders, T. M. Baumann, S. Eckart, B. Erk, A. De Fanis, K. Fehre, A. Gatton, S. Grundmann, P. Grychtol, A. Hartung, M. Hofmann, M. Ilchen, C. Janke, M. Kircher, M. Kunitski, X. Li, T. Mazza, N. Melzer, J. Montano, V. Music, G. Nalin, Y. Ovcharenko, A. Pier, N. Rennhack, D. E. Rivas, R. Dörner, D. Rolles, A. Rudenko, P. Schmidt, J. Siebert, N. Strenger, D. Trabert, I. Vela-Perez, R. Wagner, T. Weber, J. B. Williams, P. Ziolkowski, L. P. H. Schmidt, A. Czasch, K. Ueda, F. Trinter, M. Meyer, P. V. Demekhin and T. Jahnke, *Phys. Rev. Lett.*, 2020, **125**, 163201.
- 344 M. Yamazaki, J. Adachi, T. Teramoto, A. Yagishita, M. Stener and P. Decleva, *J. Phys. B: At., Mol. Opt. Phys.*, 2009, **42**, 051001.
- 345 G. Nalin, K. Fehre, F. Trinter, N. M. Novikovskiy, N. Anders, D. Trabert, S. Grundmann, M. Kircher, A. Khan, R. Tomar, M. Hofmann, M. Waitz, I. Vela-Pérez, G. Kastirke, J. Siebert, D. Tsitsonis, H. Fukuzawa, K. Ueda, J. B. Williams, D. Kargin, M. Maurer, C. Küstner-Wetekam, L. Marder, J. Viehmann, A. Knie, T. Jahnke, M. Ilchen, R. Dörner, R. Pietschnig, P. V. Demekhin and M. S. Schöffler, *Phys. Chem. Chem. Phys.*, 2021, **23**, 17248–17258.
- 346 K. Fehre, F. Trinter, N. M. Novikovskiy, S. Grundmann, D. Tsitsonis, S. Eckart, L. Bauer, M. Hilzinger, T. Jahnke, R. Dörner, P. V. Demekhin and M. S. Schöffler, *Phys. Chem. Chem. Phys.*, 2022, **24**, 13597–13604.
- 347 K. Fehre, N. M. Novikovskiy, S. Grundmann, G. Kastirke, S. Eckart, F. Trinter, J. Rist, A. Hartung, D. Trabert, C. Janke, G. Nalin, M. Pitzer, S. Zeller, F. Wiegandt, M. Weller, M. Kircher, M. Hofmann, L. P. H. Schmidt, A. Knie, A. Hans, L. B. Ltaief, A. Ehresmann, R. Berger, H. Fukuzawa, K. Ueda, H. Schmidt-Böcking, J. B. Williams, T. Jahnke, R. Dörner, M. S. Schöffler and P. V. Demekhin, *Phys. Rev. Lett.*, 2021, **127**, 103201.
- 348 K. Fehre, S. Eckart, M. Kunitski, C. Janke, D. Trabert, J. Rist, M. Weller, A. Hartung, L. P. H. Schmidt and T. Jahnke, *J. Phys. Chem. A*, 2019, **123**, 6491–6495.
- 349 J. B. Williams, C. S. Trevisan, M. S. Schöffler, T. Jahnke, I. Bocharova, H. Kim, B. Ulrich, R. Wallauer, F. Sturm, T. N. Rescigno, A. Belkacem, R. Dörner, T. Weber, C. W. McCurdy and A. L. Landers, *Phys. Rev. Lett.*, 2012, **108**, 233002.
- 350 A. Menssen, C. S. Trevisan, M. S. Schöffler, T. Jahnke, I. Bocharova, F. Sturm, N. Gehrken, B. Gaire, H. Gassert, S. Zeller, J. Voigtsberger, A. Kuhlins, F. Trinter, A. Gatton, J. Sartor, D. Reedy, C. Nook, B. Berry, M. Zohrabi, A. Kalinin, I. Ben-Itzhak, A. Belkacem, R. Dörner, T. Weber, A. L. Landers, T. N. Rescigno, C. W. McCurdy and J. B. Williams, *J. Phys. B: At., Mol. Opt. Phys.*, 2016, **49**, 055203.
- 351 E. Plésiat, P. Decleva and F. Martín, *Phys. Rev. A*, 2013, **88**, 063409.
- 352 H. Fukuzawa, R. R. Lucchese, X.-J. Liu, K. Sakai, H. Iwayama, K. Nagaya, K. Kreidi, M. S. Schöffler, J. R. Harries, Y. Tamenori, Y. Morishita, I. H. Suzuki, N. Saito and K. Ueda, *J. Chem. Phys.*, 2019, **150**, 174306.
- 353 H. Fukuzawa, S. Yamada, Y. Sakakibara, T. Tachibana, Y. Ito, T. Takanashi, T. Nishiyama, T. Sakai, K. Nagaya, N. Saito, M. Oura, M. Stener, P. Decleva and K. Ueda, *J. Chem. Phys.*, 2019, **151**, 104302.
- 354 F. Ota, K. Hatada, D. Sébilleau, K. Ueda and K. Yamazaki, *J. Phys. B: At., Mol. Opt. Phys.*, 2021, **54**, 084001.
- 355 F. Ota, K. Yamazaki, D. Sébilleau, K. Ueda and K. Hatada, *J. Phys. B: At., Mol. Opt. Phys.*, 2021, **54**, 024003.
- 356 L. Kaiser, K. Fehre, N. M. Novikovskiy, J. Stindl, D. Tsitsonis, G. Gopakumar, I. Unger, J. Söderström, O. Björneholm, M. Schöffler, T. Jahnke, R. Dörner, F. Trinter and P. V. Demekhin, *J. Phys. B: At., Mol. Opt. Phys.*, 2020, **53**, 194002.
- 357 A. Landers, Th Weber, I. Ali, A. Cassimi, M. Hattass, O. Jagutzki, A. Nauert, T. Osipov, A. Staudte, M. H. Prior,



- 427 C. I. Blaga, J. Xu, A. D. DiChiara, E. Sistrunk, K. Zhang, P. Agostini, T. A. Miller, L. F. DiMauro and C. D. Lin, *Nature*, 2012, **483**, 194–197.
- 428 Z. Chen, A.-T. Le, T. Morishita and C. D. Lin, *J. Phys. B: At., Mol. Opt. Phys.*, 2009, **42**, 061001.
- 429 C. D. Lin, A.-T. Le, Z. Chen, T. Morishita and R. Lucchese, *J. Phys. B: At., Mol. Opt. Phys.*, 2010, **43**, 122001.
- 430 Y. Ito, C. Wang, A.-T. Le, M. Okunishi, D. Ding, C. D. Lin and K. Ueda, *Struct. Dyn.*, 2016, **3**, 034303.
- 431 Y. Ito, R. Carranza, M. Okunishi, R. R. Lucchese and K. Ueda, *Phys. Rev. A*, 2017, **96**, 053414.
- 432 M. G. Pullen, B. Wolter, A.-T. Le, M. Baudisch, M. Hemmer, A. Senftleben, C. D. Schröter, J. Ullrich, R. Moshhammer, C. D. Lin and J. Biegert, *Nat. Commun.*, 2015, **6**, 7262.
- 433 B. Wolter, M. G. Pullen, A.-T. Le, M. Baudisch, K. Doblhoff-Dier, A. Senftleben, M. Hemmer, C. D. Schröter, J. Ullrich and T. Pfeifer, *Science*, 2016, **354**, 308–312.
- 434 K. Amini, M. Sclafani, T. Steinle, A.-T. Le, A. Sanchez, C. Müller, J. Steinmetzer, L. Yue, J. R. Martínez Saavedra, M. Hemmer, M. Lewenstein, R. Moshhammer, T. Pfeifer, M. G. Pullen, J. Ullrich, B. Wolter, R. Moszynski, F. J. García de Abajo, C. D. Lin, S. Gräfe and J. Biegert, *Proc. Natl. Acad. Sci. U. S. A.*, 2019, **116**, 8173–8177, DOI: [10.1073/pnas.1817465116](https://doi.org/10.1073/pnas.1817465116).
- 435 E. T. Karamatskos, G. Goldsztejn, S. Raabe, P. Stammer, T. Mullins, A. Trabattioni, R. R. Johansen, H. Stapelfeldt, S. Trippel, M. J. J. Vrakking, J. Küpper and A. Rouzée, *J. Chem. Phys.*, 2019, **150**, 244301.
- 436 W. Xie, J. Yan, M. Li, C. Cao, K. Guo, Y. Zhou and P. Lu, *Phys. Rev. Lett.*, 2021, **127**, 263202.
- 437 X. Liu, K. Amini, T. Steinle, A. Sanchez, M. Shaikh, B. Belsa, J. Steinmetzer, A.-T. Le, R. Moshhammer and T. Pfeifer, *J. Chem. Phys.*, 2019, **151**, 024306.
- 438 B. Belsa, K. Amini, X. Liu, A. Sanchez, T. Steinle, J. Steinmetzer, A. T. Le, R. Moshhammer, T. Pfeifer, J. Ullrich, R. Moszynski, C. D. Lin, S. Gräfe and J. Biegert, *Struct. Dyn.*, 2021, **8**, 014301.
- 439 J. Xu, C. I. Blaga, K. Zhang, Y. H. Lai, C. Lin, T. A. Miller, P. Agostini and L. F. DiMauro, *Nat. Commun.*, 2014, **5**, 1–6.
- 440 A. Sanchez, K. Amini, S.-J. Wang, T. Steinle, B. Belsa, J. Danek, A. T. Le, X. Liu, R. Moshhammer, T. Pfeifer, M. Richter, J. Ullrich, S. Gräfe, C. D. Lin and J. Biegert, *Nat. Commun.*, 2021, **12**, 1520.
- 441 X. Liu, K. Amini, A. Sanchez, B. Belsa, T. Steinle and J. Biegert, *Commun. Chem.*, 2021, **4**, 154.
- 442 S. G. Walt, N. Bhargava Ram, M. Atala, N. I. Shvetsov-Shilovski, A. von Conta, D. Baykusheva, M. Lein and H. J. Wörner, *Nat. Commun.*, 2017, **8**, 15651.
- 443 F. Brausse, F. Bach, F. Krečinić, M. J. J. Vrakking and A. Rouzée, *Phys. Rev. Lett.*, 2020, **125**, 123001.
- 444 N. Kotsina and D. Townsend, *Phys. Chem. Chem. Phys.*, 2021, **23**, 10736–10755.
- 445 N. Hartmann, G. Hartmann, R. Heider, M. Wagner, M. Ilchen, J. Buck, A. Lindahl, C. Benko, J. Grünert and J. Krzywinski, *Nat. Photonics*, 2018, **12**, 215–220.
- 446 I. Ismail, L. Journal, R. Vacheresse, J. Palaudoux, T. Marin, F. Penent and M. Simon, *Rev. Sci. Instrum.*, 2018, **89**, 113101.
- 447 B. Mignolet, R. D. Levine and F. Remacle, *J. Phys. B: At. Mol. Phys.*, 2014, **47**, 124011.
- 448 E. Plésiat, M. Lara-Astiaso, P. Decleva, A. Palacios and F. Martín, *Chem. – Eur. J.*, 2018, **24**, 12061–12070.
- 449 E. P. Månsson, S. Latini, F. Covito, V. Wanie, M. Galli, E. Perfetto, G. Stefanucci, H. Hübener, U. De Giovannini, M. C. Castrovilli, A. Trabattioni, F. Frassetto, L. Poletto, J. B. Greenwood, F. Légaré, M. Nisoli, A. Rubio and F. Calegari, *Commun. Chem.*, 2021, **4**, 73.
- 450 L. Cattaneo, L. Pedrelli, R. Y. Bello, A. Palacios, P. D. Keathley, F. Martín and U. Keller, *Phys. Rev. Lett.*, 2022, **128**, 063001.
- 451 S. M. Cavaletto, D. Keefer and S. Mukamel, *Proc. Natl. Acad. Sci. U. S. A.*, 2022, **119**, e2121383119.
- 452 L.-M. Koll, L. Maikowski, L. Drescher, T. Witting and M. J. J. Vrakking, *Phys. Rev. Lett.*, 2022, **128**, 043201.
- 453 K. Prince, E. Allaria, C. Callegari, R. Cucini, G. De Ninno, S. Di Mitri, B. Diviacco, E. Ferrari, P. Finetti and D. Gauthier, *Nat. Photonics*, 2016, **10**, 176–179.
- 454 D. You, K. Ueda, E. V. Gryzlova, A. N. Grum-Grzhimailo, M. M. Popova, E. I. Staroselskaya, O. Tugs, Y. Orimo, T. Sato, K. L. Ishikawa, P. A. Carpeggiani, T. Csizmadia, M. Füle, G. Sansone, P. K. Maroju, A. D'Elia, T. Mazza, M. Meyer, C. Callegari, M. Di Fraia, O. Plekan, R. Richter, L. Giannessi, E. Allaria, G. De Ninno, M. Trovò, L. Badano, B. Diviacco, G. Gaio, D. Gauthier, N. Mirian, G. Penco, P. R. Ribič, S. Spampinati, C. Spezzani and K. C. Prince, *Phys. Rev. X*, 2020, **10**, 031070.
- 455 R. H. Pratt, *Radiat. Phys. Chem.*, 2014, **95**, 4–13.
- 456 M. Kircher, F. Trinter, S. Grundmann, I. Vela-Perez, S. Brennecke, N. Eicke, J. Rist, S. Eckart, S. Houamer, O. Chuluunbaatar, Y. V. Popov, I. P. Volobuev, K. Bagschik, M. N. Piancastelli, M. Lein, T. Jahnke, M. S. Schöffler and R. Dörner, *Nat. Phys.*, 2020, **16**, 756–760.
- 457 O. Chuluunbaatar, S. Houamer, Yu. V. Popov, I. P. Volobuev, M. Kircher and R. Dörner, *J. Quant. Spectrosc. Radiat. Transfer*, 2021, **272**, 107820.
- 458 O. Chuluunbaatar, S. Houamer, Yu. V. Popov, I. P. Volobuev, M. Kircher and R. Dörner, *J. Quant. Spectrosc. Radiat. Transfer*, 2022, **278**, 108020.
- 459 R. Boll, J. M. Schäfer, B. Richard, K. Fehre, G. Kastirke, Z. Jurek, M. S. Schöffler, M. M. Abdullah, N. Anders, T. M. Baumann, S. Eckart, B. Erk, A. De Fanis, R. Dörner, S. Grundmann, P. Grychtol, A. Hartung, M. Hofmann, M. Ilchen, L. Inhester, C. Janke, R. Jin, M. Kircher, K. Kubicek, M. Kunitski, X. Li, T. Mazza, S. Meister, N. Melzer, J. Montano, V. Music, G. Nalin, Y. Ovcharenko, C. Passow, A. Pier, N. Rennhack, J. Rist, D. E. Rivas, D. Rolles, I. Schlichting, L. P. H. Schmidt, P. Schmidt, J. Siebert, N. Strenger, D. Trabert, F. Trinter, I. Vela-Perez, R. Wagner, P. Walter, M. Weller, P. Ziolkowski, S.-K. Son, A. Rudenko, M. Meyer, R. Santra and T. Jahnke, *Nat. Phys.*, 2022, **18**, 423–428.

